THE ASTROPHYSICAL JOURNAL, 417:127–144, 1993 November 1

ULTRAVIOLET IMAGING TELESCOPE: GLOBULAR CLUSTERS IN M31

RALPH C. BOHLIN, ERIC W. DEUTSCH, AND KERRY A. MCQUADE
Space Telescope Science Institute, 3700 San Martin Drive, Baltimore, MD 21218
JESSE K. HILL AND WAYNE B. LANDSMAN
Hughes STX, 4400 Forbes Boulevard, Lanham, MD 20706
ROBERT W. O'CONNELL
University of Virgina Astronomy Department, P.O. Box 3818, Charlottesville, VA 22903
MORTON S. ROBERTS
National Radio Astronomy Observatory, Edgemont Road, Charlottesville, VA 22903
AND
ANDREW M. SMITH AND THEODORE P. STECHER
Laboratory for Astronomy and Solar Physics, Code 680, Goddard Space Flight Center, Greenbelt, MD 20771
Received 1993 March 1; accepted 1993 April 29

ABSTRACT

Two 40′ fields of M31 observed with the Ultraviolet Imaging Telescope (UIT) during the Astro-1 mission in 1990 December are searched for known globular clusters. The flux of 20 clusters in the nucleus field and 23 clusters in the disk field are measured in a near ultraviolet (NUV ~2500 Å) bandpass. In the far-ultraviolet (FUV ~1500 Å), only four clusters are detected with certainty, and six others are possible detections.

The NUV photometry of the M31 globulars that are detected by UIT do not have a UV excess in comparison to their Galactic counterparts. The spectral energy distributions of the globular clusters from the NUV to *V* fall within the range of predictions of the Buzzoni models for a 15 Gyr old population. However, two of the three classical globular clusters with red NUV and visible colors that are detected in the FUV have a "UV upturn" with fluxes that are greater in the FUV than in the NUV. The other seven FUV detections have optical colors that are too blue for classical globular clusters and are probably the nuclei of compact OB associations.

Subject headings: galaxies: individual (M31) — globular clusters: general — ultraviolet: galaxies

1. INTRODUCTION

Globular clusters contain large fractional populations of cool stars and horizontal branch stars, but stars hotter than 15,000 K often contribute a large fraction of the UV flux. The temperatures of cluster stars in the core helium-burning phase (i.e., the horizontal branch) or in the subsequent double-shell source phases (post-HB) will be high, if their envelope masses are small enough. Horizontal branch stars provide valuable constraints on the global age and chemical composition of clusters. The existence of unusual temperature distributions on the HB (the "second parameter effect") provided the first good evidence for an age spread among globulars in our Galaxy (Searle & Zinn 1978; Rood & Crocker 1989; Lee, Demarque, & Zinn 1990). The post-HB phases are among the least-explored segments of the life cycle of low-mass stars and are important tracers of the production of white dwarfs (e.g., de Boer 1987). Another motivation for studying such hot objects in clusters is to understand their connection to the still-mysterious "UV-upturn" population, which is prominent in elliptical galaxies and spiral bulges (e.g., Burstein et al. 1988; Greggio & Renzini 1990; O'Connell 1993).

These hot phases normally do not contribute a large fraction of a cluster's luminosity at optical and IR wavelengths. For instance, the hot HB produces no more than ~10% of the integrated optical light (Buzzoni 1989). On the other hand, hot objects dominate the FUV light at $\lambda < 2000$ Å. Therefore, the UV is the only practical means of studying the HB and hot post-HB phases in the globular cluster systems of most external galaxies.

During the Astro-1 Spacelab mission in 1990 December, two fields in the Andromeda galaxy (M31) were imaged in the vacuum ultraviolet with the Ultraviolet Imaging Telescope (UIT). This paper presents ultraviolet photometry of previously identified globular clusters in these fields and compares our results to photometry of Galactic globular clusters.

The existing vacuum UV observations of Galactic globulars from *OAO*, *ANS*, and *IUE* indicate that there is a general correlation between the log of the relative metal abundance, [Fe/H], and UV flux in the sense that metal-deficient objects are bluer, i.e., relatively more UV bright (van Albada, de Boer, & Dickens 1981; de Boer 1985; Castellani & Cassatella 1987). However, the modest amount of available data suggests that the bluest objects may have intermediate values of [Fe/H] ~ −1.5 (de Boer 1985), rather than extremely low values. With [Fe/H] ~ −0.7, 47 Tuc is faint below 2000 Å; but the sample of such metal-rich objects is small because of large extinction in their directions. There is preliminary evidence for a small population of hot-HB or post-HB stars in three other metal-rich clusters (Rich, Minniti, & Liebert 1993). Evidently, more than one parameter affects the UV brightness of clusters. The classic "second parameter" for the HB may be involved. However, the "blue" HB stars that participate in the second parameter effect are often too cool ($T \sim 10{,}000$–$13{,}000$ K) to contribute much FUV light. The scatter in the FUV observations could be produced by the presence or absence of a few very hot objects on the HB or in hot post-HB phases. Dynamical evolution of clusters could also be involved (Djorgovski & Piotto 1993).

The rich M31 globular cluster system presents the opportunity to study the populations of clusters with a wide range of metal abundance and relatively low and uniform foreground extinction. In general, optical spectroscopy indicates that the M31 and Galactic cluster systems are similar. However, the more metal-rich clusters show line strength anomalies with respect to Galactic globulars in the Balmer series, CN, Ca II, and Sr II (Spinrad & Schweizer 1972; O'Connell 1983; Burstein et al. 1984; Tripicco 1989; Brodie & Huchra 1991). Interpretation of these differences is controversial. Burstein et al. (1984) and Tripicco (1989) have argued that the M31 objects are significantly younger than the Galactic clusters; but differences in relative abundances, i.e., different [X/Fe], cannot be ruled out. Earlier rocket UV and *IUE* measurements of M31 globular clusters (see § 3) are affected by low signal-to-noise. This paper reports the most sensitive upper limits and the first reliable fluxes for M31 clusters in the FUV.

2. OBSERVATIONS AND DATA ANALYSIS

2.1. *Observations*

Of the 17 exposures taken with the UIT of M31, only the six longest exposures listed in Table 1 are used in this study. Each of the fields was digitized, linearized, and flat-fielded as described in Stecher et al. (1992). The two far-UV (FUV) nucleus fields are registered and co-added. This combined image is the basis for all subsequent analysis. The registration is accomplished by a simple translation of a few pixels and is accurate to $\sim 1''$. The limiting sensitivity of the co-added image improves only 17% with respect to the single longer exposure, rather than the 32% that is predicted from the total of the two exposure times. In one case, the uncertain detection of Bo86 on the co-added frame contrasts with the appearance of a definite detection on the single frame FUV266. For a flat spectrum, the near-UV (NUV) A1 filter is centered at 2490 Å with a bandwidth of 1150 Å; the FUV B1 filter is centered at 1520 Å with a bandwidth of 354 Å. The diameter of the point spread function (PSF) at 50% enclosed energy is 7″–8″ in the NUV and $11'' \pm 2''$ in the FUV for the M31 images, while a Gaussian fit to the sharp cores of the stellar profiles has a full width at half maximum of $\sim 3''$ for most UIT frames.

2.2. *Search and Identification*

The two NUV images are searched for all class A and B clusters from Battistini et al. (1987, hereafter BoII, Bologna group). The two groups of clusters "include all the nonstellar objects with regular, circular, symmetric brightness distributions" (BoII). The majority of these candidates have been confirmed as clusters by spectroscopic observations (Huchra, Stauffer, & van Speybroeck 1982). Of these ~ 350 class A and B clusters, about 150 are within our fields of view. For each cluster whose coordinates are within the fields, the immediate vicinity is examined in conjunction with a similar portion of a digitized Guide Star Selection System (GSSS) image (Lasker et al. 1990). Of the ~ 150 possible clusters, only the 42 entries (excluding vdB0) in Table 2 are detectable in one or both of the two NUV fields (Figs. 1 and 2). While six of the seven clusters in the overlap region are detected in only the deeper disk frame, Bo110 is detected in both fields, so that 41 distinct clusters with Bo numbers are detected. UV/optical finding charts for the individual clusters are provided in Figure 3. The detected clusters are enclosed by a 20″ diameter circle on the UIT image and companion GSSS image. The position of each circle is determined by the astrometry for the image and the corresponding coordinate in Table 2.

The UIT images contain many local fluctuations in the background noise, which must not be mistaken for sources. The finding chart in Figure 3 for Bo60 provides a typical example of the problems involved in finding faint sources. By using local offset stars visible in both the UIT and GSSS image, we confirm the identification of Bo60 in the UIT image to 2″.5. The "object" just north of the cluster is probably just a dust particle on the film. In general, the GSSS images are used to confirm the identification to less than 3″. In addition, a dewarping technique is used to correct for the typical 10″–20″ distortions in the UIT image intensifier tubes and again confirm our identifications to $\sim 3''$. One exception is Bo212 at the edge of the field, where the center of the circle in Figure 3 is 4″.5 from the object.

Finally, using the list of globular clusters found in the NUV, the FUV fields are searched within the small search radius of 5″ that is allowed by the FUV dewarping astrometry. Only the brightest NUV sources are detectable in the FUV images. Nine clusters are detected in the FUV images, along with the open cluster vdB0. The FUV fluxes are in Table 3 and the finding charts appear in Figure 4.

2.3. *Detection Limits*

To estimate a detection limit for the UIT images, measurements for several apertures are centered on 50 different "clear noise" regions. A histogram of the measurements is approximately a Gaussian distribution, from which a 3 σ detection threshold is estimated. The detection limits calculated in this way are in Table 4. These limits are observational fluxes and include no extinction corrections. Adding synthetic stars to a clean noise field yields the same detection threshold to within 20%. A similar detection threshold can also be calculated from a typical rms scatter of $\sim 10^{-18}$ ergs s^{-1} cm^{-2} Å^{-1} pixel^{-1}, where the object radius is 15 pixels and the background annulus is between 15 and 25 pixel radii. The UIT plate scale is 1″.14 per pixel. Some cluster positions have a limit brighter by a few 0.1 mag due to high local noise or artifacts, as is the case for the seven upper limit entries in Table 3.

2.4. *UV Photometry*

Because the local sky background in the UIT images of M31 is not uniform in the region surrounding many of the clusters, automated aperture photometry of faint sources has large errors. Instead, background values and PSF fits to the clusters are determined in conjunction with a visual inspection of each object to identify and reject artifacts. Globular clusters in M31 have typical diameters of less than 2″ (Cowley & Burstein 1988, hereafter CB) and have the same PSF as stars.

Aperture photometry is computed for each identified cluster for a range of circular apertures of radius 3 to 25 pixels. The

TABLE 1

ULTRAVIOLET IMAGING TELESCOPE FIELDS USED IN THIS STUDY

Field	UIT ID	RA (2000)	DEC	Exp. (s)	Filt.
Nucleus	NUV 236	00 42 37.1	+41 13 22	330	A1
Nucleus	FUV 266	00 42 37.1	+41 13 22	384	B1
Nucleus	FUV 293	00 42 37.1	+41 13 22	286	B1
Disk	NUV 387	00 41 27.4	+40 50 39	116	A1
Disk	NUV 388	00 41 27.4	+40 50 39	583	A1
Disk	FUV 485	00 41 27.4	+40 50 39	582	B1

TABLE 2

NEAR-ULTRAVIOLET CLUSTER PHOTOMETRY

Bo # (1)	ALT ID (2)	α (2000) (3)	δ (2000)	f_{249}^a (4)	σ^a (5)	m_{249} (6)	[Fe/H] (7)	V (8)	$B-V$ (9)	$E(B-V)$ (10)	M_v (11)	$(m_{249}-V)_o$ (12)
Nucleus field												
23	G78	00 41 1.2	+41 13 45	13.2	3.4	18.60	−0.92	14.26	1.13	0.31	−10.92	3.36
64	G125	00 42 2.0	+41 11 7	20.6	3.4	18.12	−1.55	16.44	0.85	0.10	−8.07	1.36
70:	G133	00 42 6.9	+41 07 55	15.2	3.4	18.45		16.88[c]	0.71[c]	0.10	−7.63	1.25
86	G148	00 42 18.6	+41 14 1	51.6	3.6	17.12	−1.74	15.04	0.75	0.10	−9.47	1.76
103	G165	00 42 29.7	+41 17 57	13.0	4.2	18.62	−0.56	15.17[d]	1.01[d]	0.10	−9.34	3.13
107	G169	00 42 31.2	+41 19 39	16.0	4.4	18.39	−1.18	15.96[d]	0.89[d]	0.10	−8.55	2.11
110	G172	00 42 33.1	+41 03 28	21.9	3.7	18.05	−1.00	15.22	0.89	0.24	−9.74	2.00
114:	G175	00 42 34.3	+41 12 44	5.5	3.4	19.66		17.05[e]	1.01[e]	0.10	−7.46	2.29
133	G191	00 42 51.6	+41 23 30	71.2	13.8	16.77		17.51[e]	0.66[e]	0.10	−7.00	−1.06
145		00 43 1.6	+41 12 26	14.1	3.8	18.53		18.10[e]		0.10	−6.41	0.11
148	G200	00 43 3.9	+41 18 4	23.8	3.2	17.96	−1.53	16.00	0.80	0.10	−8.51	1.64
151:	G205	00 43 9.6	+41 21 32	14.7	3.5	18.48	−0.75	14.83	1.27	0.34	−10.45	2.57
158	G213	00 43 14.4	+41 07 20	32.4	3.7	17.62	−1.08	14.68	0.90	0.10	−9.83	2.62
161:	G215	00 43 15.5	+41 11 24	12.5	3.5	18.48	−1.25	16.11	0.82	0.10	−8.40	2.05
165:	G218	00 43 18.3	+41 10 54	8.7	4.1	18.66	−1.80	16.19	0.76	0.10	−8.32	2.15
171:	G222	00 43 25.6	+41 15 37	19.2	5.1	18.19	−0.48	15.22	0.98	0.10	−9.29	2.65
178	G229	00 43 30.9	+41 21 16	61.8	4.4	16.92	−1.51	15.04	0.79	0.10	−9.47	1.56
179	G230	00 43 31.2	+41 18 14	20.6	4.2	18.12	−1.21	15.24	0.84	0.10	−9.27	2.56
182:	G233	00 43 36.7	+41 08 12	14.6	5.1	18.19	−1.19	15.38	0.96	0.26	−9.64	1.99
212	G263	00 44 3.2	+41 04 57	26.8	6.0	17.83	−1.75	15.58	0.70	0.10	−8.93	1.93
Disk field												
322	G49	00 40 17.2	+40 39 6	39.3	2.3	17.41		17.92[f]	−0.08[f]	0.10	−6.59	−0.83
327	G53	00 40 24.0	+40 36 22	108.3	14.5	16.31		16.61	0.32	0.10	−7.90	−0.62
338	G76	00 40 58.8	+40 35 47	87.1	3.6	16.55	−1.34	14.26	0.84	0.10	−10.25	1.97
341:	G81	00 41 9.0	+40 35 53	2.8	1.9	20.28		16.38	0.92	0.10	−8.13	3.58
25:	G84	00 41 12.6	+41 00 28	4.4	2.5	19.79		16.81[g]	0.91[g]	0.10	−7.70	2.66
27	G87	00 41 14.6	+40 55 51	15.2	2.1	18.45	−1.64	15.63	0.84	0.10	−8.88	2.50
28	G88	00 41 16.5	+40 59 3	7.5	2.4	19.21		16.81[g]	0.93[g]	0.10	−7.70	2.08
342	G94	00 41 24.0	+40 36 46	12.9	2.1	18.62		18.35	0.06	0.10	−6.16	−0.05
34	G96	00 41 28.1	+40 53 49	8.8	2.5	19.04	+0.31	15.53	0.90	0.10	−8.98	3.19
40	G102	00 41 38.9	+40 40 53	21.0	1.9	18.09		17.46[b]	0.38[b]	0.10	−7.05	0.31
43	G106	00 41 42.3	+40 42 38	30.6	2.2	17.68	−2.13	16.96	0.26	0.10	−7.55	0.40
58	G119	00 41 53.0	+40 47 8	35.2	2.1	17.53	−1.45	15.04	0.82	0.10	−9.47	2.17
60	G121	00 41 57.0	+41 05 13	15.7	2.4	18.41		16.64	0.40	0.10	−7.87	1.45
66	G128	00 42 3.0	+40 44 45	25.6	2.5	17.88		17.42	0.36	0.10	−7.09	0.14
67:	G129	00 42 3.1	+41 04 23	5.9	3.6	19.47		17.24[b]	0.87[b]	0.10	−7.27	1.91
73:	G134	00 42 7.3	+40 59 21	6.6	3.4	19.35	−0.64	15.99	0.92	0.10	−8.52	3.04
76:	G138	00 42 10.2	+41 05 21	10.8	2.2	18.82	−1.35	16.88[g]	0.84[g]	0.10	−7.63	1.62
81	G142	00 42 13.6	+40 48 38	10.0	4.5	18.90		16.72[g]	0.63[g]	0.10	−7.79	1.86
85	G147	00 42 18.3	+40 39 57	7.3	2.2	19.24	−1.83	16.84	0.71	0.10	−7.67	2.08
110	G172	00 42 33.1	+41 03 28	24.9	2.4	17.91	−1.00	15.22	0.89	0.24	−9.74	1.93
111:	G173	00 42 33.1	+41 00 26	9.2	3.1	18.99		16.82	0.69	0.10	−7.69	1.85
117	G176	00 42 34.3	+40 57 9	6.2	2.8	19.42	−1.75	16.36	0.76	0.10	−8.15	2.74
vdB0		00 40 29.4	+40 36 14[h]	674.0	21.1	14.28		15.05	0.22	0.10	−9.46	−1.09

[a] Flux in units of 10^{-17} ergs s^{-1} cm^{-2} Å^{-1}.
[b] Sharov & Lyuty 1985.
[c] Sharov et al. 1984.
[d] Sharov et al. 1992.
[e] Crampton et al. 1985.
[f] BoII.
[g] Sharov et al. 1987.
[h] Coordinates for vdB0 are from our measurement of the GSSS image and should be accurate to ~2″–3″. The coordinates of Crampton et al. 1985 agree in right ascension but are off 16″ toward the south. The coordinates of Hodge 1992 agree with ours in declination but are off 2^s toward the west.

aperture corrections are defined by the mean PSF of bright star images. The dominant uncertainty is often the sky background level. However, the photometric accuracy is improved by our technique of choosing a sky value which produces a constant aperture corrected flux level for all aperture sizes. Local features in M31 and film artifacts are taken into account when determining the proper background value. The cluster flux is the average of the aperture corrected photometry for radii between 3 and 15 pixels; the uncertainty is the rms scatter among the 13 separate flux determinations. The aperture correction is determined from the integrated flux of the PSF versus radius. A 15 pixel aperture is the standard size for the UIT absolute calibration that is based on *IUE* spectra of stars in some UIT images. The overall statistical uncertainty is the combination in quadrature of this rms scatter with one-third of the 3 σ basic detection limit of the plate (see Table 4 and § 2.3), because the uncertainty due to sky noise is always present, even if the net signal above sky fits the PSF perfectly with zero

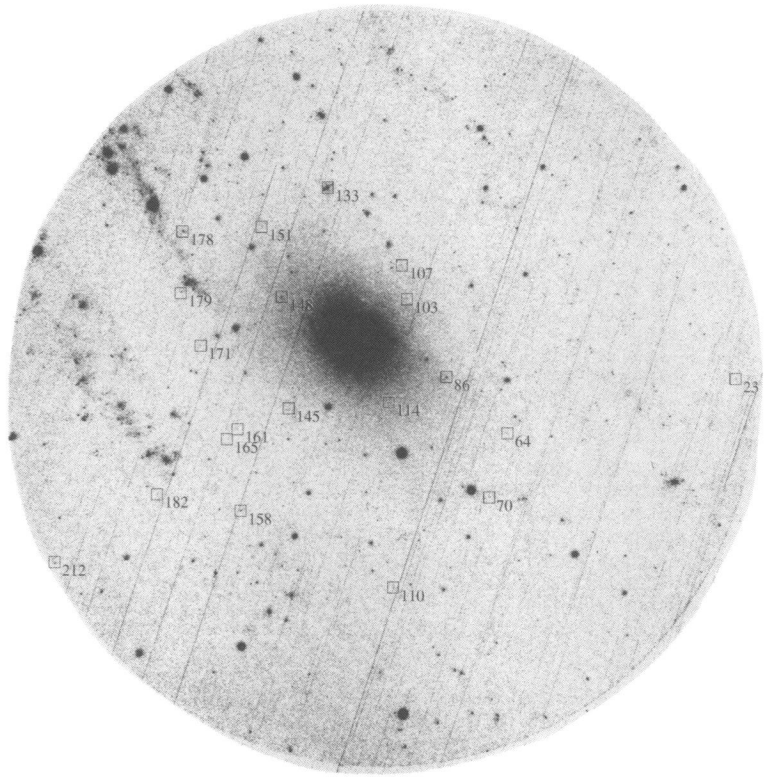

FIG. 1.—Near-UV M31 nucleus image with the detected Bologna group (Bo) globular clusters enclosed by squares. The full UIT field of ~40′ is shown. North is at the top; east is to the left.

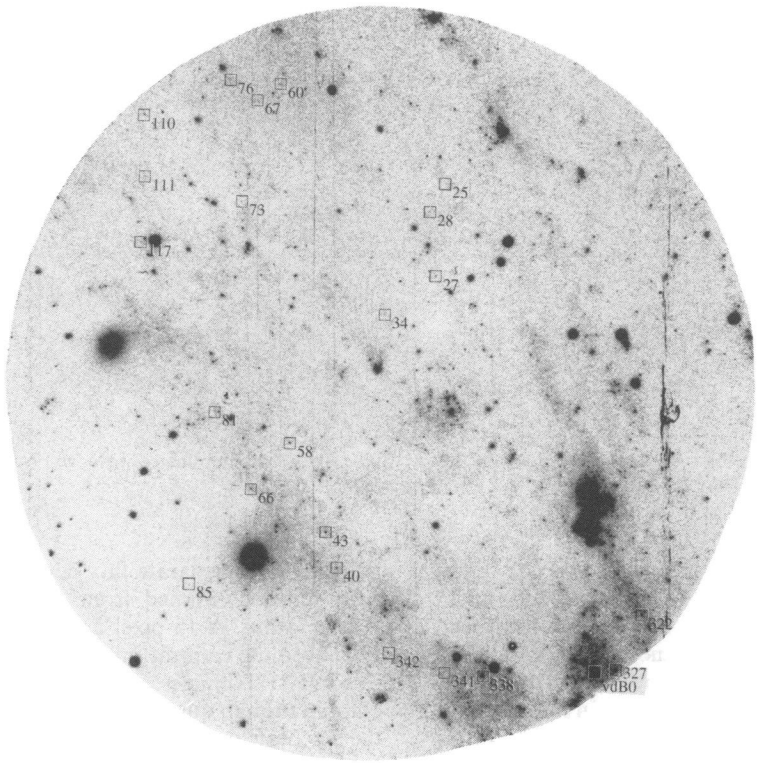

FIG. 2.—Same as for Fig. 1 in the disk image

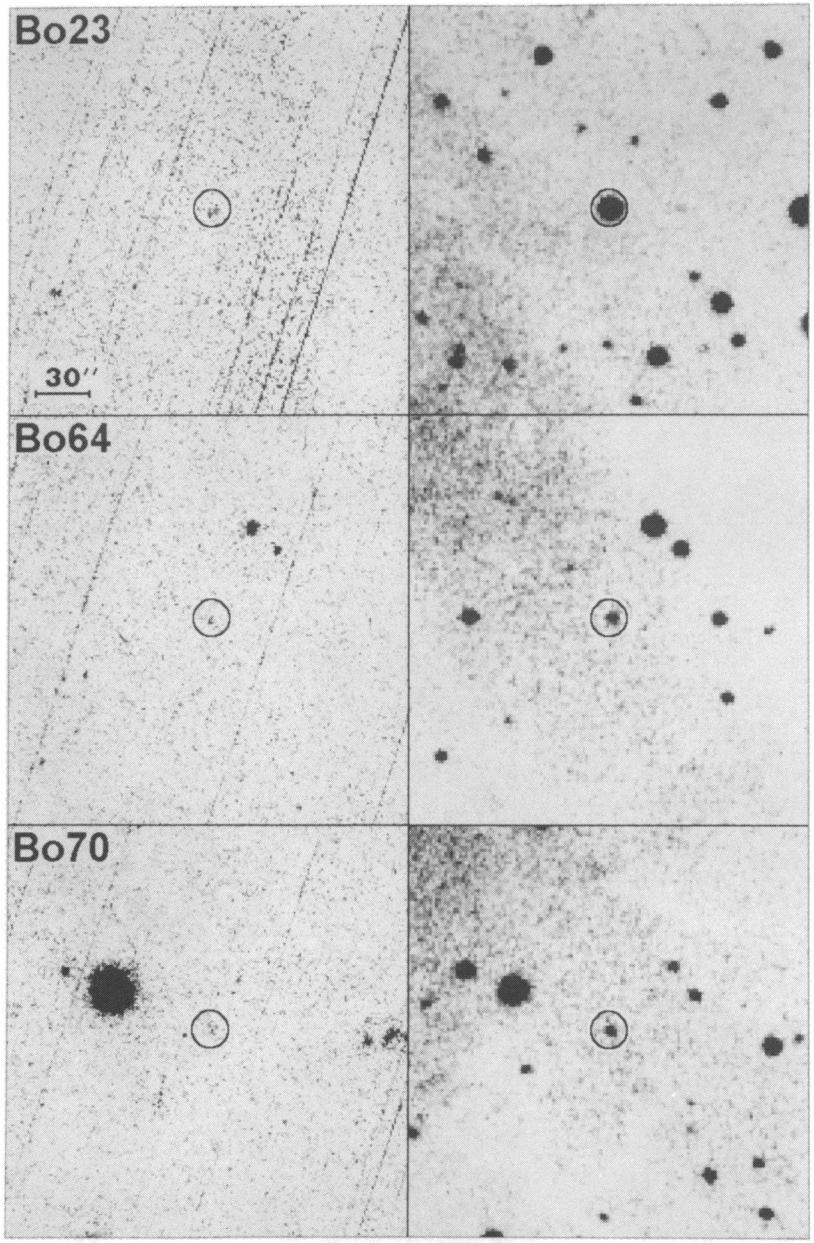

FIG. 3A1

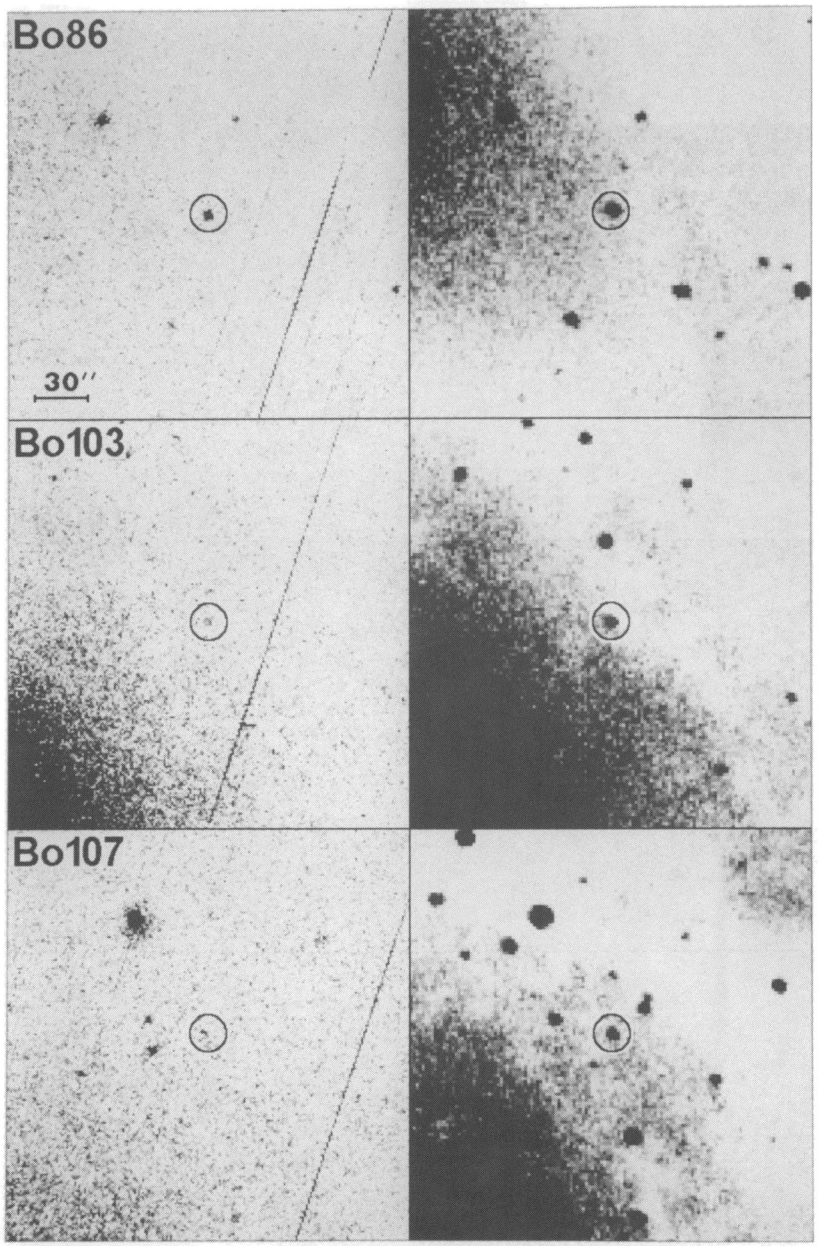

FIG. 3A2

FIG. 3.—Finding charts with north up and east to the left for the detected Bo clusters from Table 2 in the (*a*) nucleus field followed by those in the (*b*) disk field. For each cluster, the NUV sub-field of 3′.8 × 3′.8 is shown adjacent to the corresponding GSSS field with the same scale. The 20″ diameter circle is placed at the coordinates in Table 2 per the astrometry for each image. The clusters are usually centered in the circle to less than 3″ in both cases.

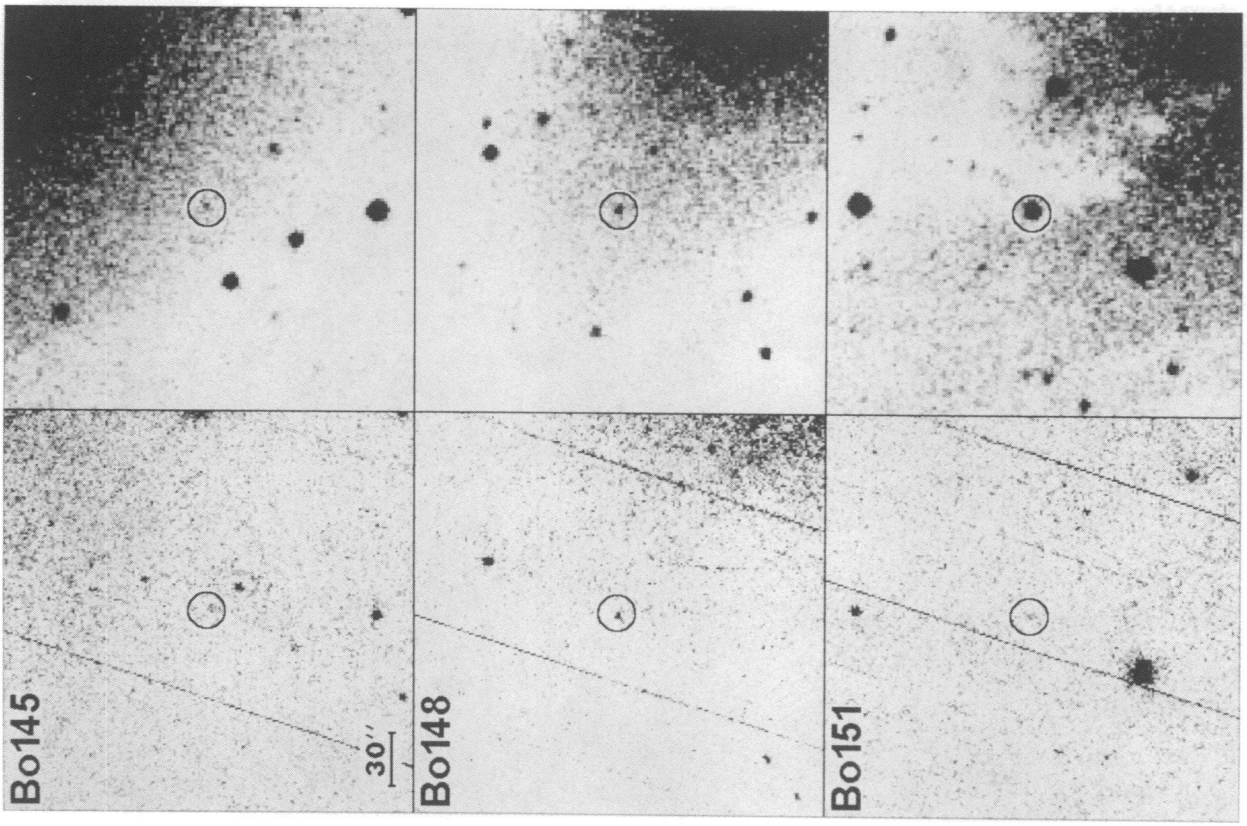

FIG. 3A4

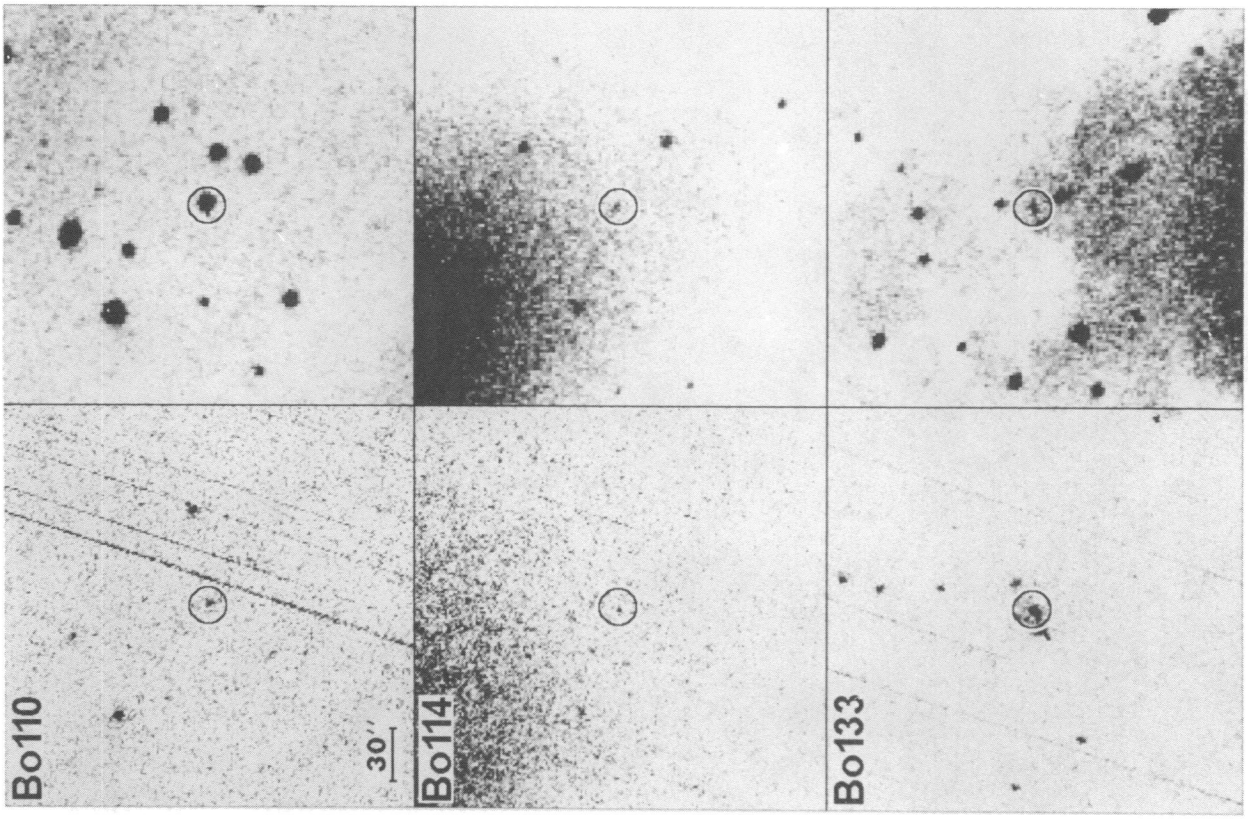

FIG. 3A3

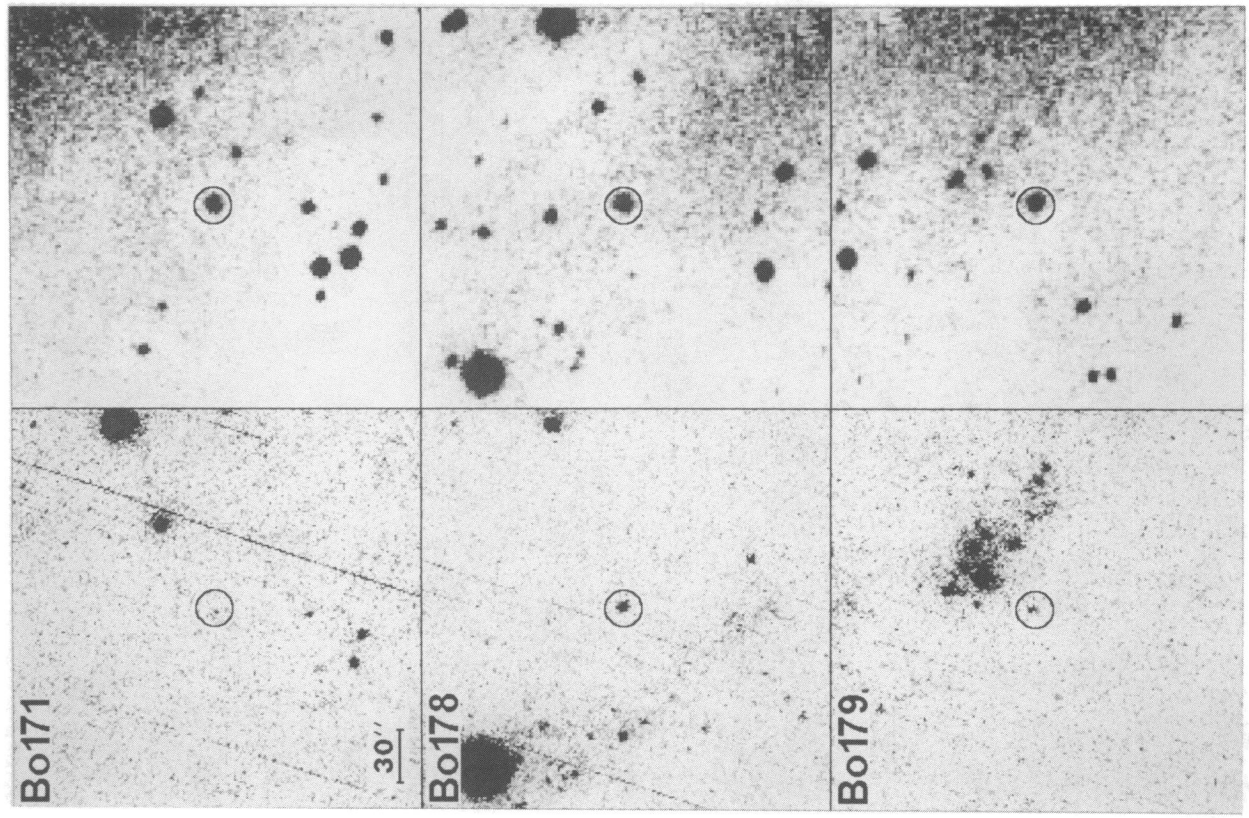

FIG. 3A6

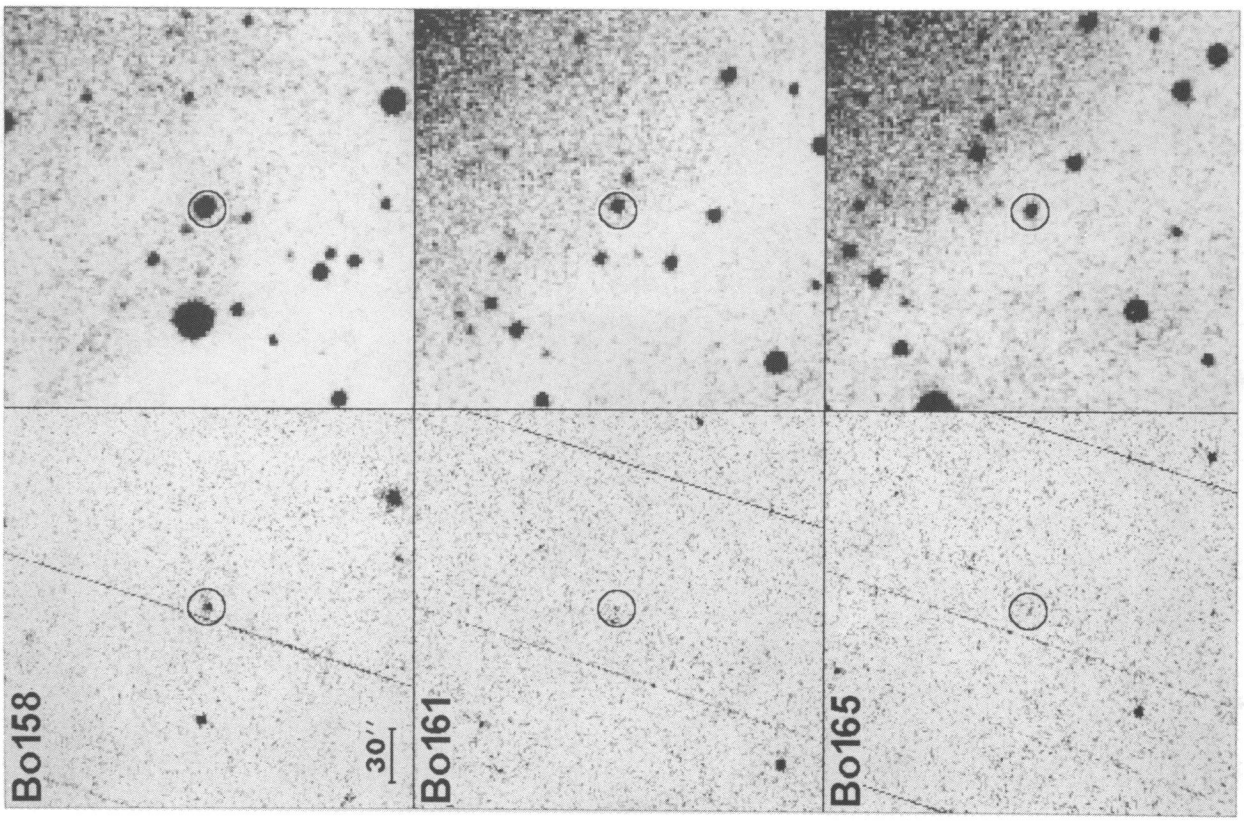

FIG. 3A5

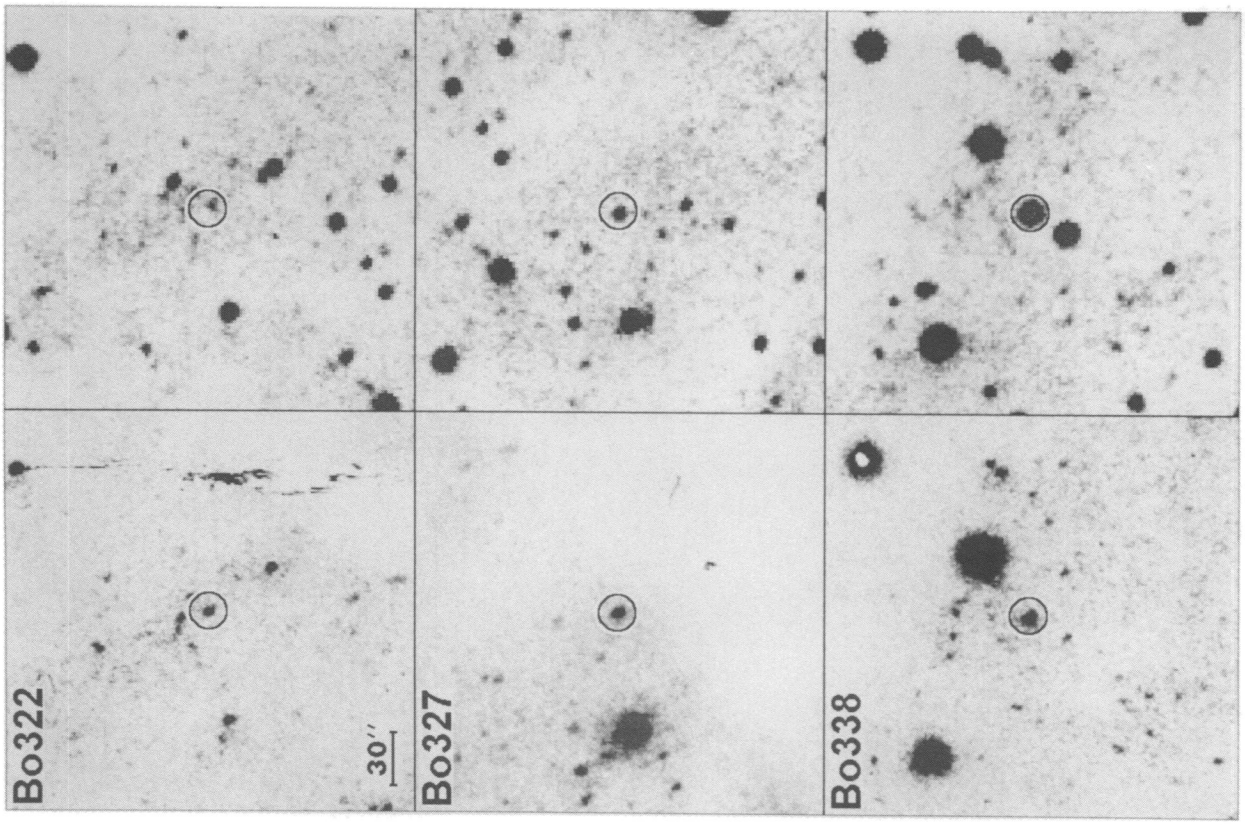

FIG. 3B1

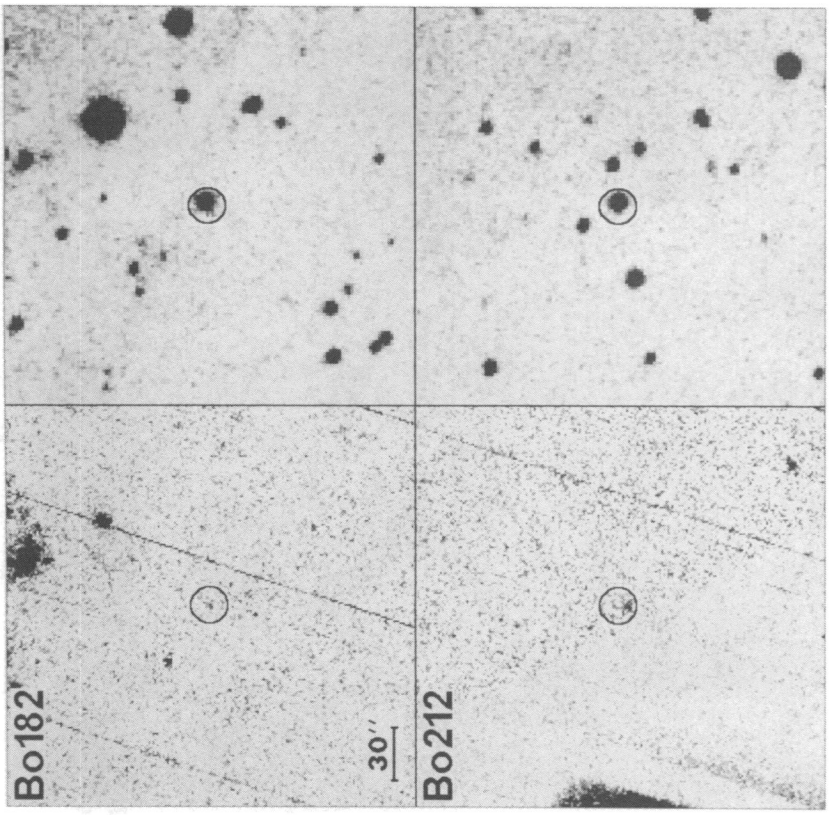

FIG. 3A7

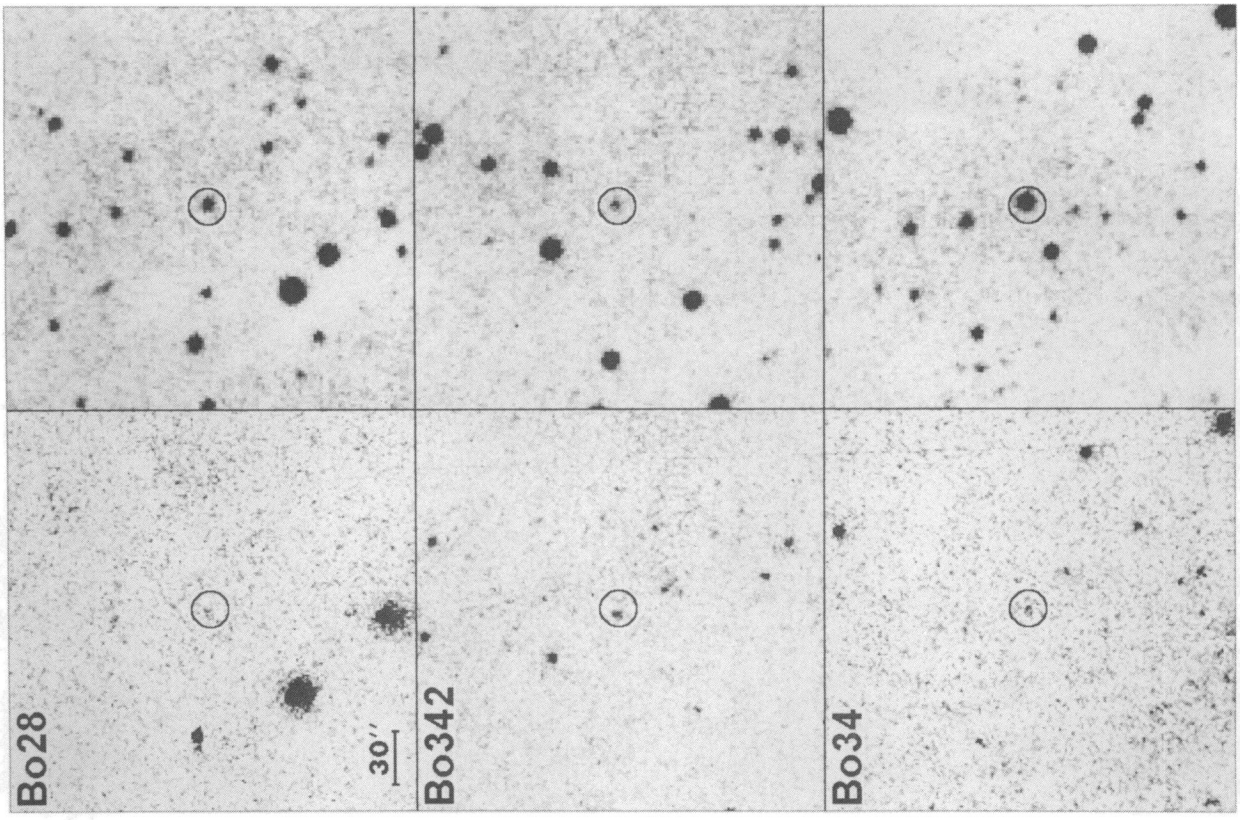

FIG. 3B3

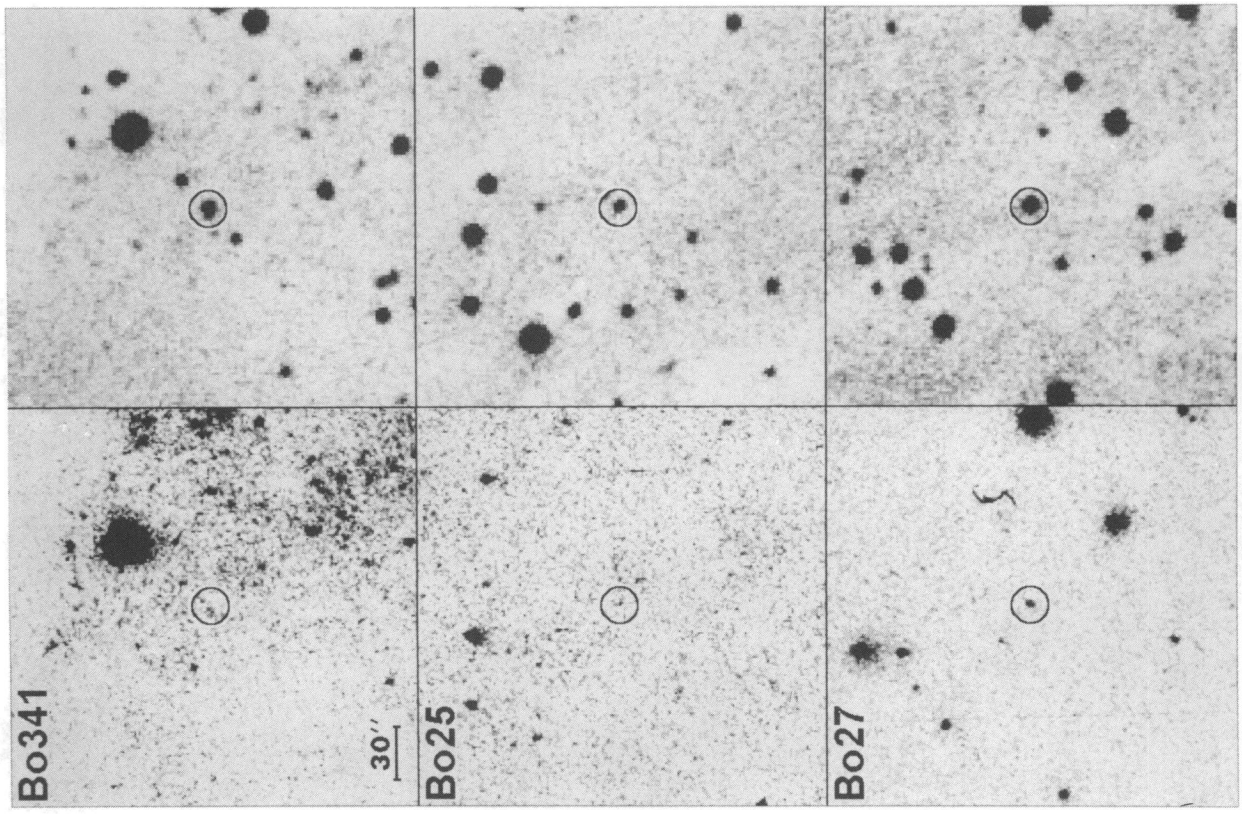

FIG. 3B2

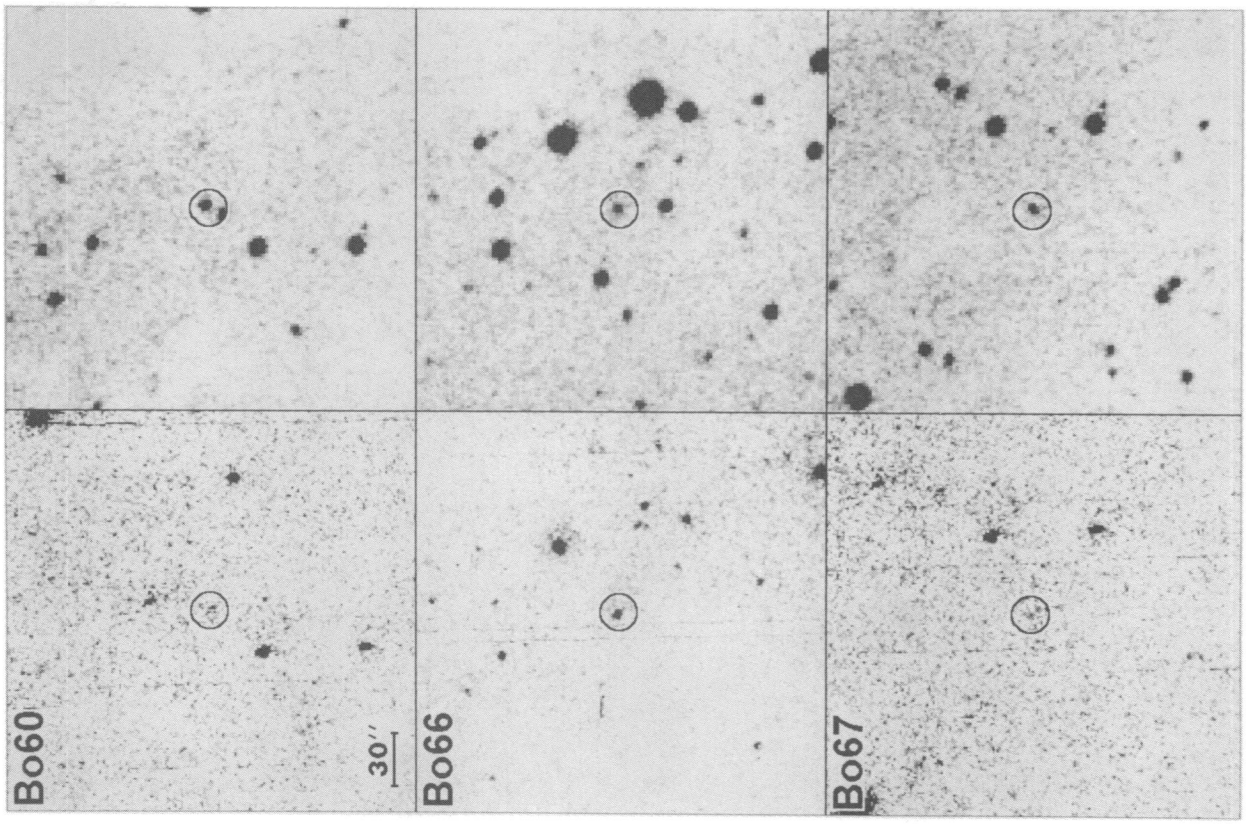

FIG. 3B5

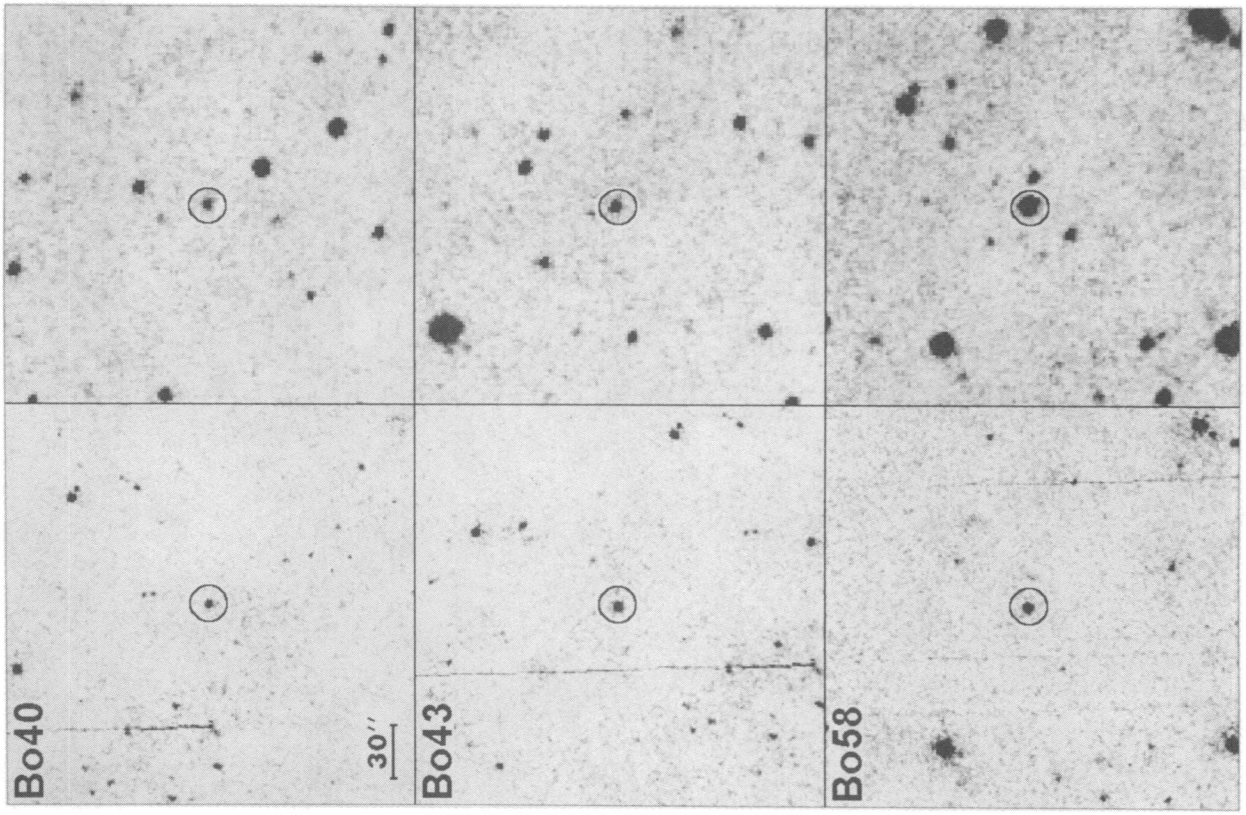

FIG. 3B4

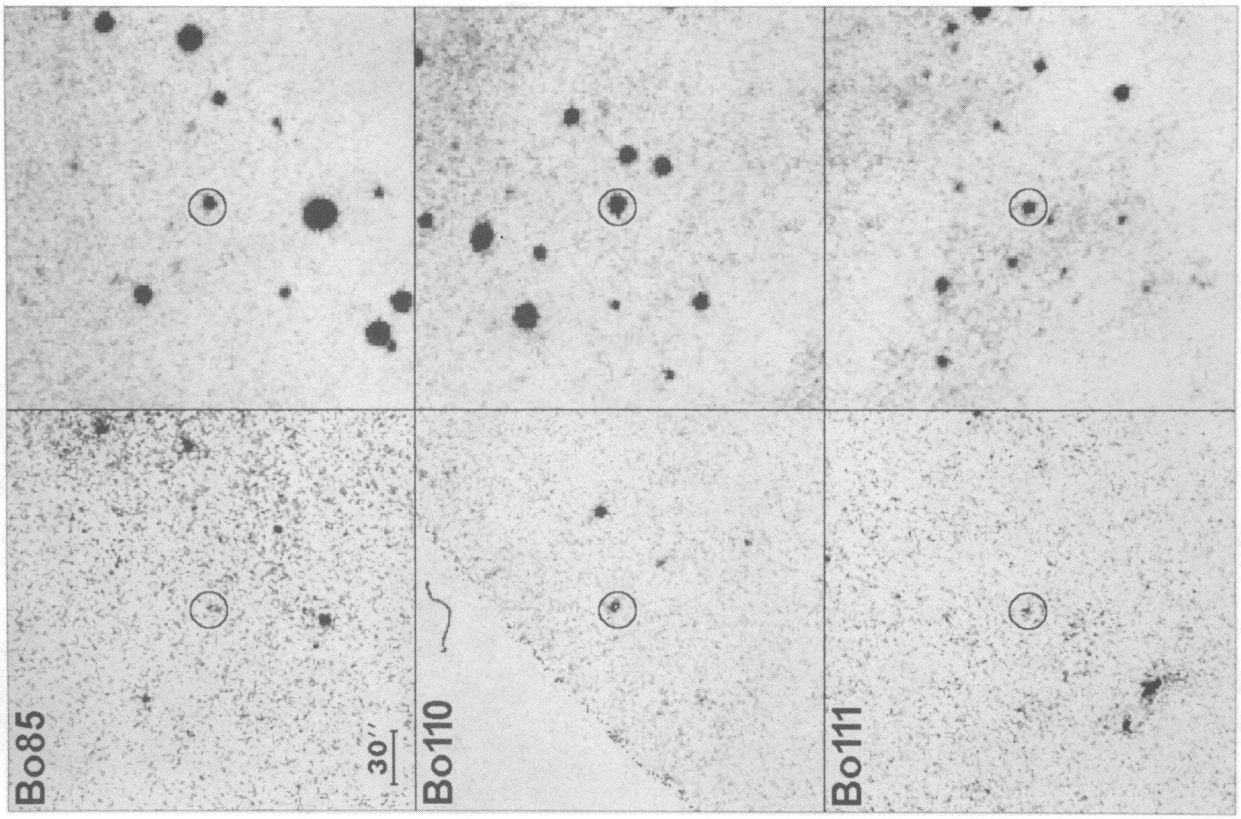

FIG. 3B7

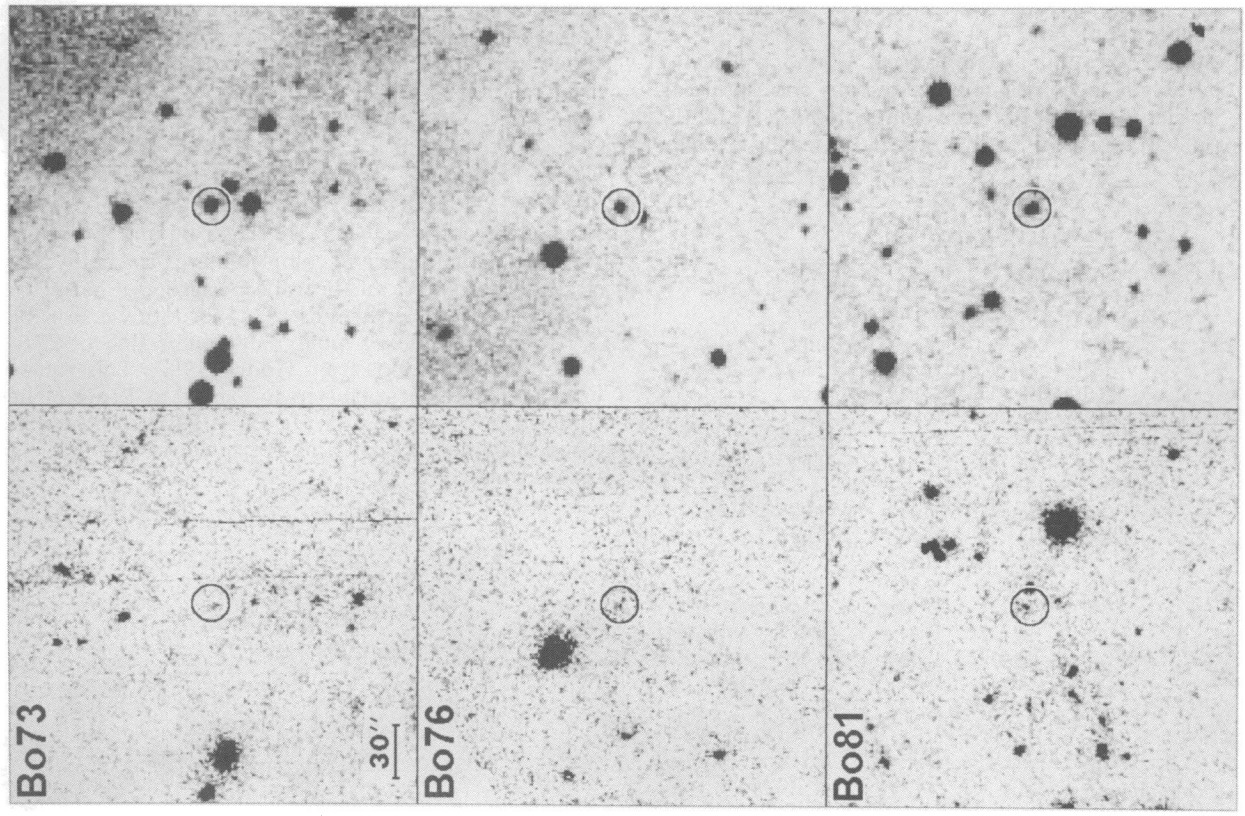

FIG. 3B6

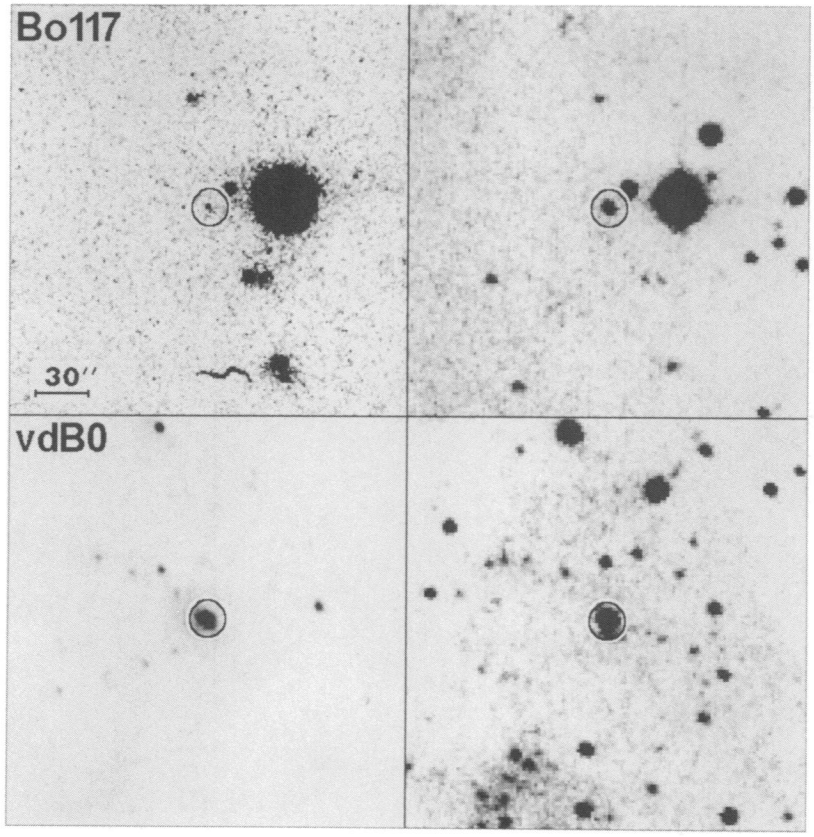

FIG. 3B8

rms scatter. In addition to the statistical uncertainty, there is an estimated systematic absolute calibration uncertainty of ~15% (Stecher et al. 1992).

Our photometric results are in Table 2. For each detected cluster, the Bologna Group ID number and any corresponding ID from Sargent et al. (1977) are given in columns (1) and (2). The more uncertain identifications are indicated by a colon following the Bo ID. Coordinates from BoII are given in column (3). Columns (4) and (5) give our observed fluxes and the overall 1 σ statistical uncertainties. The fluxes are converted into monochromatic magnitudes in column (6) using the usual relation

$$m_{249} = -2.5 \log (f_{249}) - 21.1 ,$$

where the flux f_{249} is in units of ergs s^{-1} cm^{-2} $Å^{-1}$ for the NUV A1 filter. The metallicities in column (7) are from Huchra, Brodie, & Kent (1991). Columns (8) and (9) are observed magnitudes and colors and are principally the photoelectric photometry of the Moscow group (Sharov & Lyuty 1983) and other references listed in the footnotes to Table 2.

The standard foreground reddening value of $E(B-V) = 0.10$ in column (10) is from Hodge (1992). This value is confirmed for eight of the clusters in Table 2 by Frogel, Persson, & Cohen (1980), while a larger $E(B-V)$ is indicated for four cases. Column (11) contains the intrinsic absolute V-magnitude calculated by

$$M_V = V - 24.19 - A_V ,$$

TABLE 3

FAR-ULTRAVIOLET CLUSTER PHOTOMETRY

Bo #	f_{152}^a	σ^a	m_{152}	$(m_{152}-V)_o$
Nucleus Field				
67	<33	21	>17.60	> −0.13
86:	56	11	17.03	1.50
110	<56	14	>17.03	>0.63
133	178	27	15.77	−2.23
148	<30	8	>17.71	>1.22
178	<38	20	>17.45	>1.92
Disk Field				
322	95	17	16.46	−1.95
338:	46	17	17.23	2.48
27	<38	9	>17.44	>1.25
342:	55	9	17.05	−1.79
40:	39	11	17.41	−0.54
43:	47	8	17.23	−0.22
58	<40	11	>17.39	>1.86
66	82	17	16.62	−1.29
85:	20	11	18.14	0.81
117	<25	14	>17.90	>1.05
vdB0	1233	79	13.67	−1.87

[a] Units of 10^{-17} ergs s^{-1} cm^{-2} $Å^{-1}$.

TABLE 4

DETECTION LIMITS

Field	Bandpass	Limiting Flux[a]	Magnitude
Nucleus	NUV	7.6×10^{-17}	19.2
Nucleus	FUV	15.1×10^{-17}	18.4
Disk	NUV	5.2×10^{-17}	19.6
Disk	FUV	21×10^{-17}	18.1

[a] Units of ergs s^{-1} cm^{-2} $Å^{-1}$.

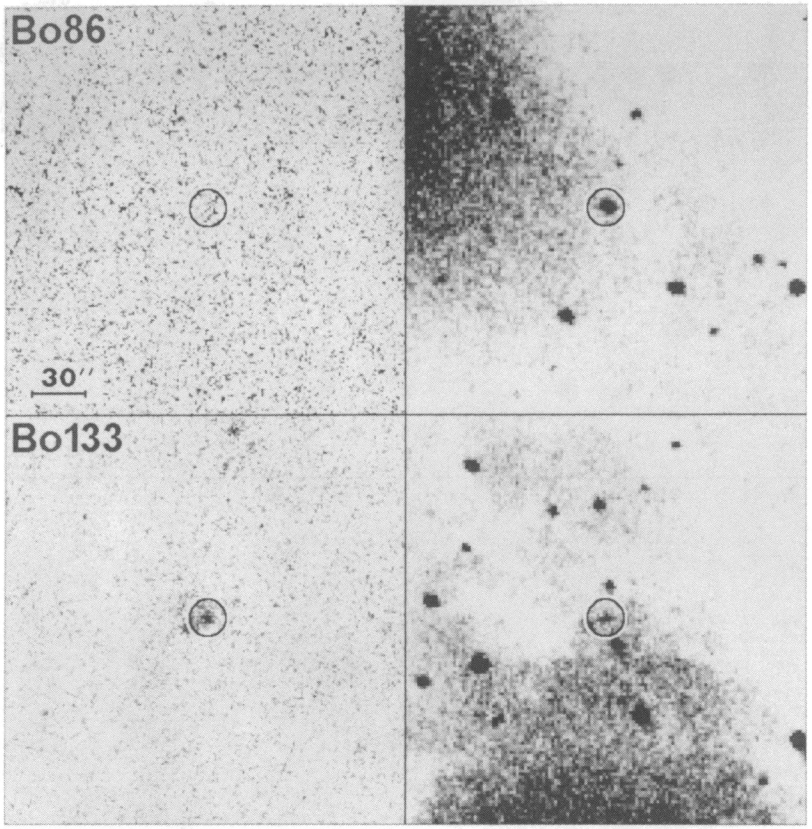

FIG. 4A1

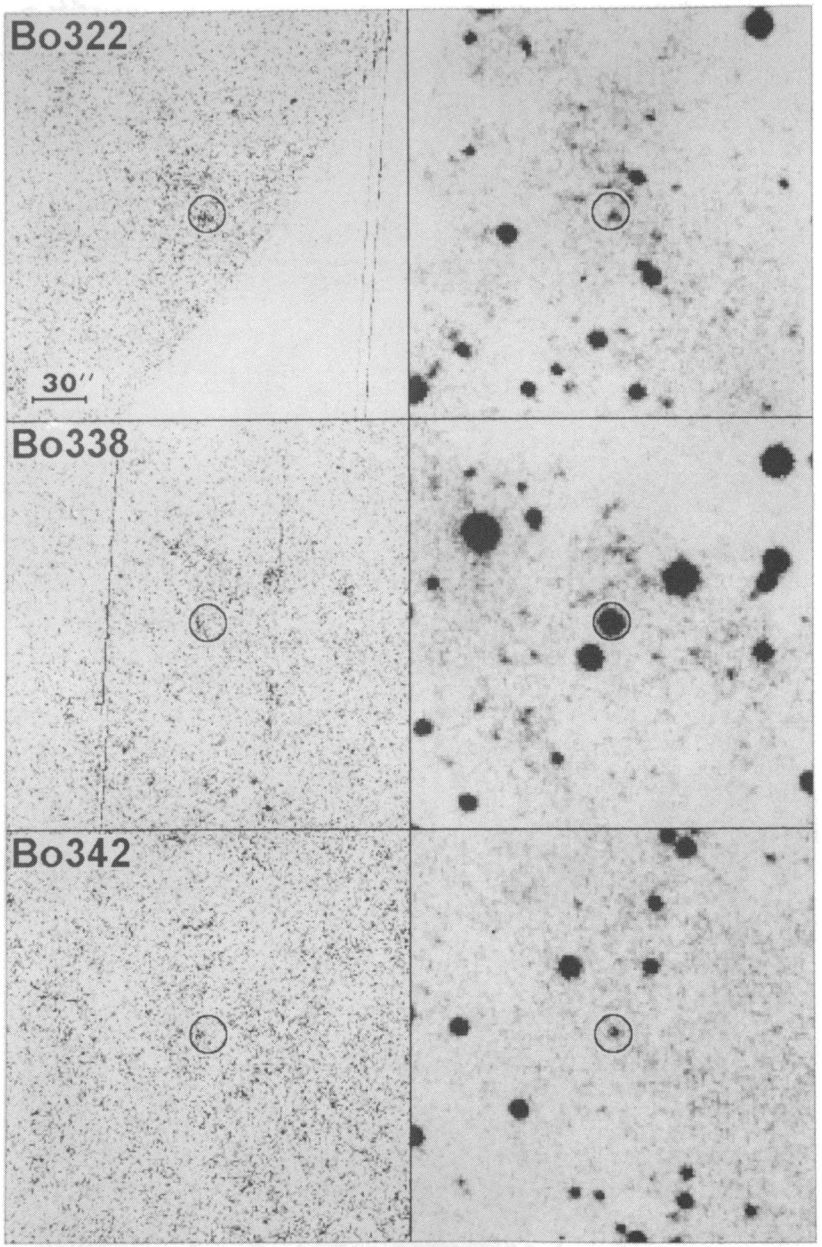

FIG. 4B1

FIG. 4.—Same as for Figure 3 for the detected clusters in the FUV from Table 3

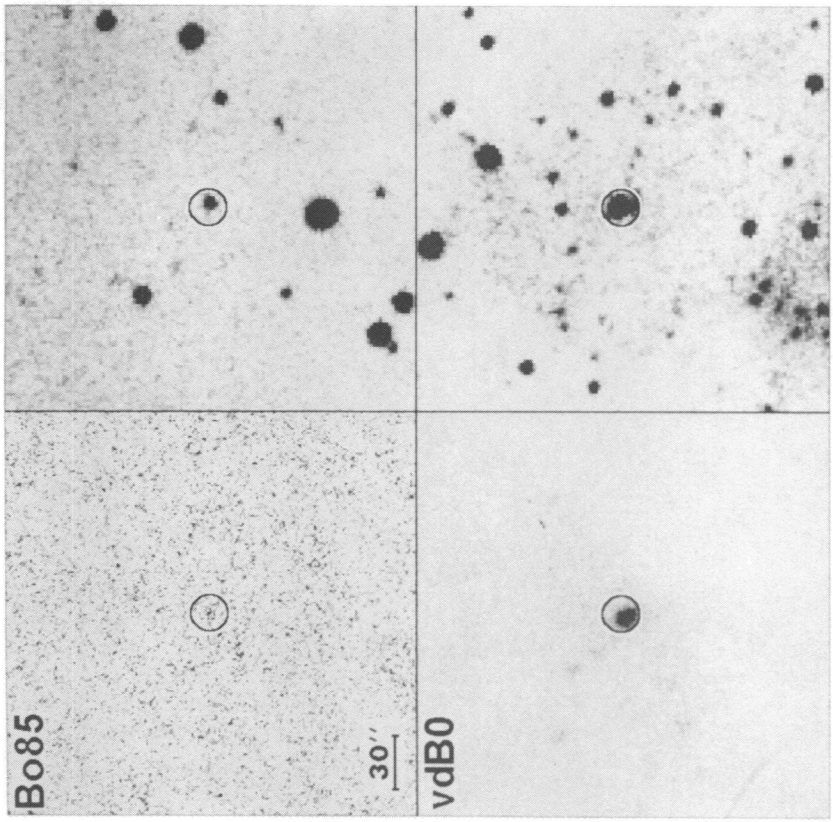

FIG. 4B3

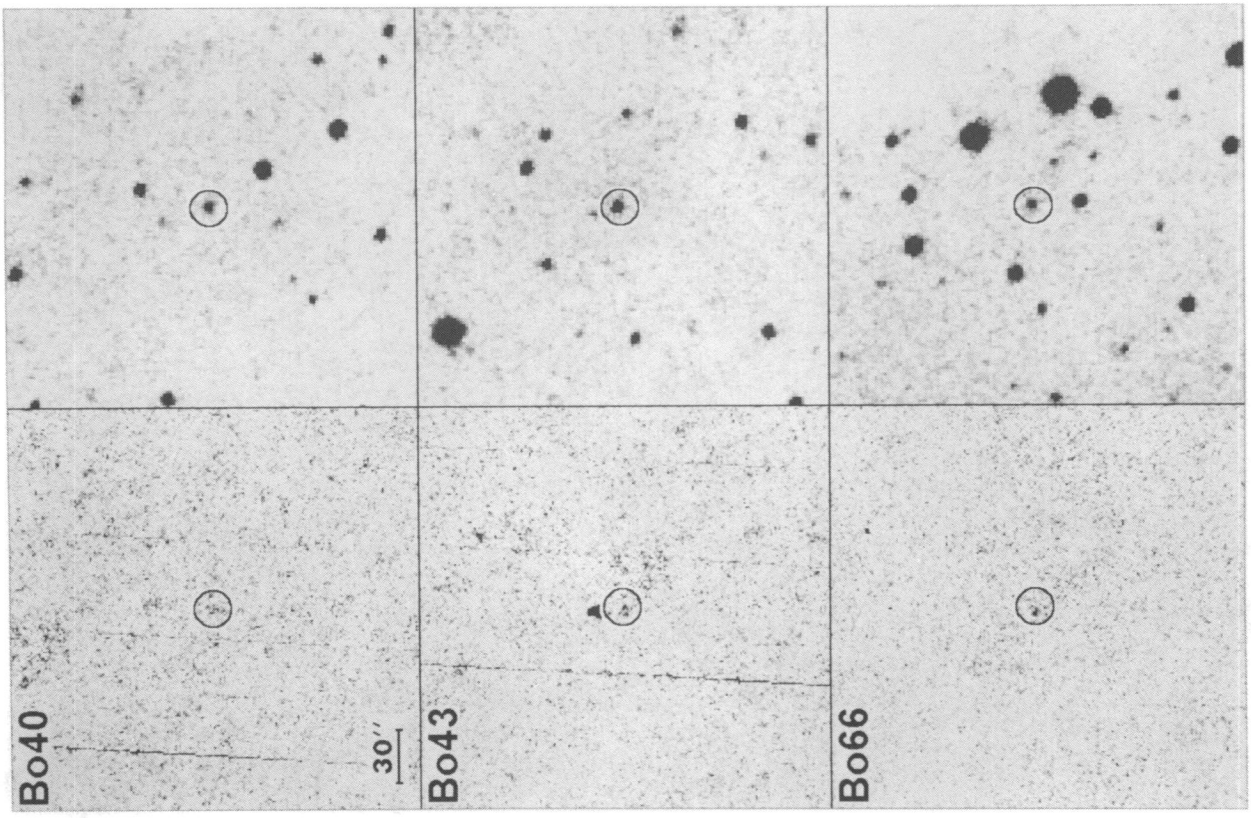

FIG. 4B2

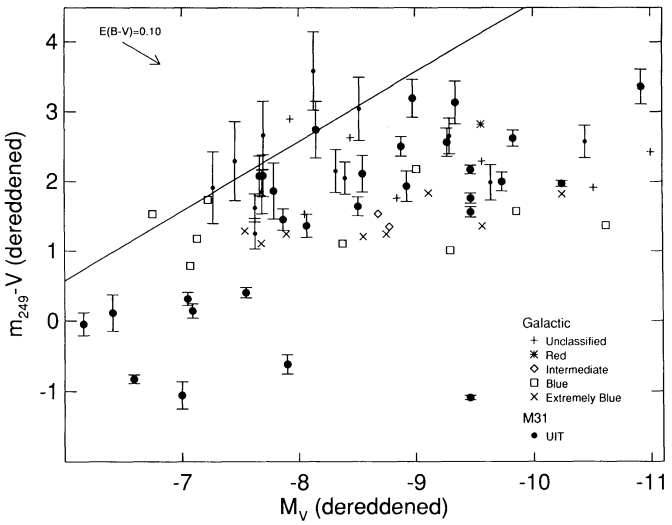

FIG. 5.—M_V vs. $(m_{249} - V)_0$ diagram for M31 and Galactic globular clusters. The smaller filled circles are the uncertain UIT detections that are indicated by a colon in Table 2. Galactic globular clusters are coded by the symbols indicated on the figure for the different UV color classes of van Albada (1981). The arrow represents the shift produced by an increase of 0.10 in the reddening parameter $E(B-V)$. The sloping straight line is our 3 σ detection limit for $m_{249} = 19.4$ and $E(B-V) = 0.1$. The error bars on the data points are 1 σ uncertainties.

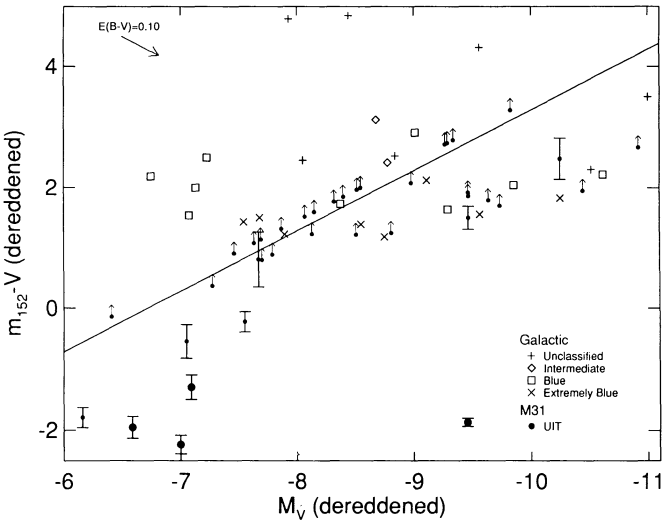

FIG. 6.—Same as in Figure 5, except for $(m_{152} - V)_0$ from Table 3. The FUV detection limit is for $m_{152} = 18.2$. Only cluster detections in the NUV are shown. Upper limits and uncertain detections are indicated by the smaller filled circles.

where 24.19 is our adopted distance modulus (Elson & Walterbos 1988) and $A_V = 3.2E(B-V)$. The reddening function of Seaton (1979) is used at all wavelengths. Finally, the dereddened $(m_{249} - V)_0$ values are listed in column (12). Our m_{249} values have been dereddened using $A_{NUV} = 6.4E(B-V)$. Although 2490 Å is the effective wavelength of the NUV A1 filter for flat spectra, 2700 Å is the effective wavelength of the A1 filter for an average Galactic globular cluster spectrum from *ANS* observations. This method of dereddening the NUV fluxes is accurate to ~ 0.05 mag for $E(B-V) = 0.1$.

Figure 5 is a color versus absolute magnitude plot, based on the two last columns in Table 2 in conjunction with similar values for Galactic globular clusters. The Galactic sample is the intersection of the objects in Harris & Racine (1979), which provides the integrated M_V, and the objects in de Boer (1985), which contains total UV flux values from scaled *ANS* observations. The flux values used for the Galactic globular clusters are derived by convolving approximate energy distributions from the multiwavelength *ANS* observations with the NUV A1 transmission curve. The UV color classifications are based on *ANS* photometry from van Albada et al. (1981). Since the Galactic classes are based on FUV − NUV colors from *ANS*, the locations of the *ANS* data in Figures 5–7 are not always perfectly correlated with the expected color code rank.

Table 3 contains the FUV photometry and dereddened $(m_{152} - V)_0$ colors for the 10 clusters that are detected in the FUV frames and the seven clusters that have poorer upper limits than the general limits of Table 4. The extinction at 1520 Å for the FUV B1 filter is $A_{FUV} = 8.1E(B-V)$ for the Seaton (1979) reddening function. Since the spectrum of the typical globular cluster in de Boer (1985) is flat over the B1 filter, the nominal effective wavelength of 1520 Å is the appropriate mean wavelength for the dereddening. Figure 6 compares the intrinsic FUV colors for the M31 clusters with the intrinsic colors of Galactic globular clusters. The Galactic data is *ANS* photometry at 1550 Å from the same references as in Figure 5. Seven of the 10 clusters that are detected in the FUV, including the bright blue object (vdB0) at $M_V \sim -9.5$, are members of the "blue group" discussed in § 4.1. Bo327 is our brightest globular cluster in the NUV but is just off the FUV field of view.

3. DISCUSSION

3.1. *Comparison with Earlier Rocket-UV Photometry*

3.1.1. *NUV*

An earlier UV imaging study of the M31 clusters (Bohlin et al. 1988) employed a rocket prototype of the UIT to obtain 15″

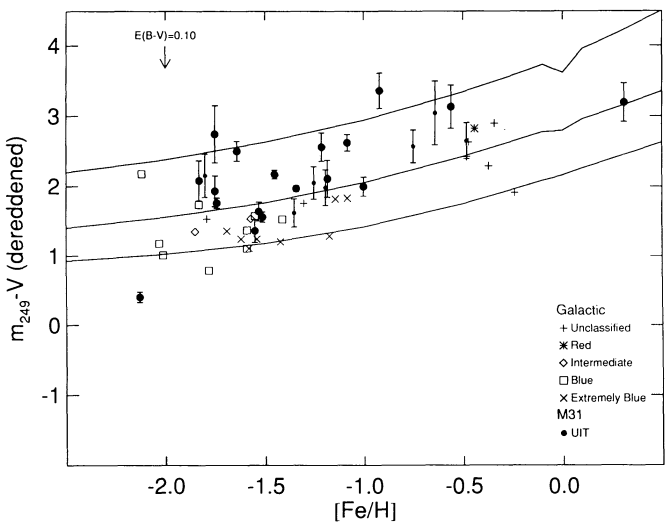

FIG. 7.—Metallicity index [Fe/H] vs. the intrinsic $(m_{249} - V)_0$ for 25 globular clusters observed by UIT and 23 Galactic clusters measured by *ANS*. M31 clusters are indicated by filled circles with error bars. The solid lines are the predictions of the Kurucz (1992) model atmospheres for effective temperatures 5000, 5500, and 6000 K, respectively from the top. The effect on any data point of a dereddening of $E(B-V) = 0.1$ is indicated by the length of the arrow.

resolution imagery with a detection threshold of $m_\lambda(2500\ \text{Å}) \sim 19$. Of the 17 globular clusters discussed in that rocket paper, 15 are within the UIT fields of view. Four of these are not present in the NUV UIT images, even though our detection limit is fainter than all but the magnitude of Bo157 quoted in the 1988 paper. Reexamination of the old rocket image suggests that these four unconfirmed detections could be background noise clumps. There are similar enhancements of the background noise in the rocket image which do not correspond to any visual or UIT soures. The agreement of the 11 NUV magnitudes that are common to both papers is better than 0.4 mag for nine of these and better than 0.6 mag for Bo64 and Bo327. The rocket paper gives a 16.9 ± 0.2 magnitude for Bo327, while our magnitude is 16.3 ± 0.2. This difference is significant at only the 2 σ level. Both papers also include a NUV flux measurement for the open cluster vdB0; however, our measurement is 1.4 mag brighter. The lack of saturation in the NUV388 image of vdB0 is confirmed by the photometry from the shorter exposure NUV387.

3.1.2. *FUV*

The same 15 clusters, except Bo327, also fall within the UIT FUV fields. While the UIT data produce upper limits for 12, the rocket paper for the faint clusters are up to 0.7 mag brighter than the more reliable UIT values, the rocket flux for the bright vdB0 is 1 mag fainter than the UIT magnitude. There may be some undetected nonlinearity in the old rocket photometry of vdB0.

3.2. *Comparison with IUE Observations*

Four of the clusters in our fields have been observed by *IUE*. Crotts et al. (1990) used a "specialized reduction procedure" for faint *IUE* spectra to derive the UV fluxes of Bo58 (V23). Our fluxes in units of ergs s^{-1} cm^{-2} $Å^{-1}$ for Bo58 of 3.5×10^{-16} in the NUV and our upper limit of 2.1×10^{-16} in the FUV agree with the *IUE* fluxes of $\sim 5 \times 10^{-16}$ at 2500 Å and less than 3×10^{-16} at 1500 Å. For Bo158 (V64), *IUE* values of 8.1×10^{-16} at 2500 Å and 5×10^{-16} at 1500 Å were measured by Cacciari et al. (1982), according to Crotts et al. (1990). These noisy *IUE* spectra of Bo158 (LWR 8699 and SWP 10280) are reanalyzed with the optimal extraction technique of Kinney, Bohlin, & Neill (1991) in conjunction with a visual examination of the line-by-line image of the *IUE* data. Our UIT flux for Bo158 of 3.2×10^{-16} in the NUV and the upper limit of 1.5×10^{-16} in the FUV are consistent with our reanalysis of the *IUE* data. The problem with the LWR 8699 spectrum is that noise clumps on the order of 10% above background dominate the signal below about 2700 Å, while the true signal is only a few percent above the average background noise. For SWP 10280, the net signal mirrors the camera artifact spectrum of Crenshaw, Breugman, & Norman (1990), which has many features at the 10^{-15} flux level. Therefore, the *IUE* spectrum of Bo158 provides only an upper limit of about 5×10^{-16} below 2000 Å, although the image shows that a faint UV source is present near the center of the *IUE* slit.

Cowley & Burstein (1988, hereafter CB) studied *IUE* spectra of 11 M31 clusters and found that most had larger fluxes at 1500 and 2500 Å than Galactic globulars with similar optical-band colors. CB suggested that the M31 globulars were comparable to the intermediate-age clusters in the Large Magellanic Cloud and that some ages were as small as ~ 2 Gyr. However, Barbero et al. (1990) found that the UV colors of CB were not consistent with models for intermediate age populations, while Tripicco (1989) obtained high-resolution optical spectra of some of the CB clusters and was able to exclude the presence of significant hot components in two of these. CB plot the observed *IUE* fluxes for four of our clusters: Bo338 (G76, V12), Bo58 (G119, V23), Bo86 (G148, V62), and Bo158 (G213, V64). The UIT and *IUE* measurements are in agreement at NUV wavelengths, except for the case of the LWR8699 spectrum of Bo158, which is discussed above. In the FUV, our reanalysis of the *IUE* spectra is consistent with the UIT results, except for the detailed discussion of Bo338 that follows. The FUV fluxes of CB are above the levels permitted by the UIT data for all four clusters, and the SWP images for Bo58 and Bo86 do not show even the trace signal that is present for Bo158. Crotts et al. (1990) also suggested that CB made some systematic error in their data analysis, because their *IUE* spectra have no negative points. Our extractions of these SWP spectra have many noisy points that fall below the mean background level, even for the CB prescription of using the three lines of the *IUE* image that contain the bulk of the signal for the bright object Bo338. A moderate smoothing of either a three-line extraction or an optimal extraction still does not reproduce the appearance of the published CB spectra. For Bo338, our analysis of SWP 24000 produces a mean flux of 11×10^{-16} over the 1250–1950 Å range. The uncertainty of SWP fluxes is at least 5×10^{-16} because of the artifact spectrum. However, a two percent uncertainty in the background (10^{-15} in net flux units) probably dominates this noisy 4 hour exposure of Bo338, in view of the 10% undulations in the smoothed *IUE* background on the scale of 100 Å. Thus, the UIT value of $f_{152} = 5 \times 10^{-16}$ for Bo338 is also consistent with the *IUE* data for Bo338. Furthermore, the UIT flux measurement agrees with the prediction in Figure 1 of Crotts et al. (1990), while the CB value is higher than expected from the flux range of Galactic globular clusters at the distance of M31. Even Bo86, the brightest of the three classical globular clusters detected by UIT at $f_{152} = 6 \times 10^{-16}$, would produce only a poor SWP spectrum. In general, NUV detections of M31 globulars by *IUE* are confirmed; but the *IUE* fluxes in the FUV are spurious or of low reliability.

3.3. *Comparison with ANS Observations*

There are 33 globular clusters detected by UIT in M31 in the NUV frames. In addition, nine blue clusters are found with intrinsic colors $m_{249} - V < 1$, $B-V < 0.6$, and ages less than ~ 1 Gyr. All 33 of the globulars are BoII class A (certain) clusters, except for the class B (less certain) Bo158. The average intrinsic color of these 33 globulars is $\langle m_{249} - V \rangle = 2.2$, while the corresponding average of the 27 Galactic globulars of de Boer (1985) is 1.7. The difference between these mean colors may be dominated by selection effects, since the ~ 100 BoII clusters that are not detected by UIT must be fainter than our sensitivity limit in Figure 5. The *ANS* sample favored blue and UV bright globulars and, therefore, would have omitted the redder ones. The only observable differences between the M31 and *ANS* samples are at brighter values than the detection limit lines in Figures 5 and 6, where there is no evidence for the UV excess suggested by CB. On the contrary, among the classical globular clusters, which are located redward of $(B-V)_0 \sim 0.6$ in Figure 8, there are two differences between the Galactic and M31 colors. First, there is a possible deficiency in the M31 population of analogs to the blue and extremely blue Galactic clusters. Second, the body of the $m_{249} - V$ colors in M31 lies above the Galactic sample. An underestimate

in the reddening correction for a few of the M31 clusters could vitiate the first conclusion. Furthermore, both the M31 and galactic samples are subject to sampling effects, such as restricted radial distance from the galactic centers.

The FUV fluxes from UIT of two of the three classical globulars with $B-V$ redder than ~ 0.5 and $(m_{249} - V)$ redder than ~ 1.0 are at the "blue" fringe of the $(m_{152} - V)$ colors of Galactic globulars, but neither are 3 σ more UV bright than their bluest Galactic counterpart. Both of these extremely blue globulars (Bo85 and 86) are brighter in the FUV than the NUV and, thus, have a UV upturn." Our measurements or upper limits are adequate to determine that Bo 58, 158, 178, and 338 do *not* have UV upturns.

3.4. *Blue Clusters*

Nine of the detected clusters (Bo133, Bo145, Bo322, Bo327, Bo342, Bo40, Bo43, Bo66, and vdB0) have intrinsic $(m_{249} - V)_0$ colors less than 1.0, and are bluer than any Galactic globular in Figure 5. Attention was previously drawn to Bo43 and Bo327 by Bohlin et al. (1988), who suggested that they may be analogous to the LMC "blue globulars." The blue $m_{249} - V$ colors reflect ages much younger than the 15 Gyr that are typical for Galactic globulars. Ages are estimated for the blue clusters using evolutionary models of Schaller et al. (1992) with [Fe/H] $= -1.5$ and model atmospheres of Kurucz (1992). For these young clusters, the sensitivity of $m_{249} - V$ to the metallicity [Fe/H] is small. For example, a model cluster of age 100 Myr with [Fe/H] $= -1.5$ or -0.4 predicts $m_{249} - V = -1.08$ or -0.94, respectively. The initial mass function (IMF) is assumed to be a power law with exponent -1.5. The relation between the ages (t) and the NUV photometry for $t > 15$ Myr is $(m_{249} - V)_0 = -3.58 + 1.25 \log (t)$, where t is in units of 100 Myr and the range of predicted ages is 100–1500 Myr.

The modeling of the NUV photometry predicts FUV colors which tend to be redder than the observed $(m_{152} - V)_0$ colors by up to ~ 1 mag. Of the four certain FUV colors, the $(m_{152} - V)_0 = -1.29$ for Bo66 is the most discrepant from the predictions. The estimate for this value of -1.29 predicts an age of 270 Myr, rather than the 950 Myr for the age that is based on the $(m_{249} - V)_0$. More sophisticated models are needed.

There is also some question as to whether these objects are young globular clusters. Bo40, Bo43, and Bo66 are listed in Battistini et al. (1980, hereafter BoI) as being in an OB association "OB 84" but are all given class A designations in BoII. Bo322, Bo327, and Bo342 are not listed in BoI but do appear in BoII as class B clusters. *HST* imaging could resolve the proper categorization of these blue clusters from their morphology. However, eight of these blue clusters are faint with M_V between -6 and -8. As age increases, these eight should become fainter than classical globular clusters. Hodge (1992, p. 167) suggests that some of these blue objects could be "more properly considered to be nuclei of compact OB associations than stable open clusters."

3.5. *Metallicity*

Figure 7 plots $(m_{249} - V)_0$ versus the metallicity index [Fe/H] for 25 clusters observed by UIT, and 23 Galactic clusters measured by *ANS*. van Albada et al. (1981) classified the Galactic globular clusters from the *ANS* UV fluxes. Figure 7 also shows $(m_{249} - V)$ versus metallicity from the Kurucz (1992) model atmospheres for stars near the globular cluster main-sequence turnoff. The dependence of $(m_{249} - V)_0$ on line blanketing is evident, while the general agreement of the model atmosphere and the globular cluster colors suggests that stars in the effective temperature range 5000–6000 K are the primary contributors to the observed NUV flux. The blue clusters of § 4.1 are hotter but do not have published [Fe/H] values.

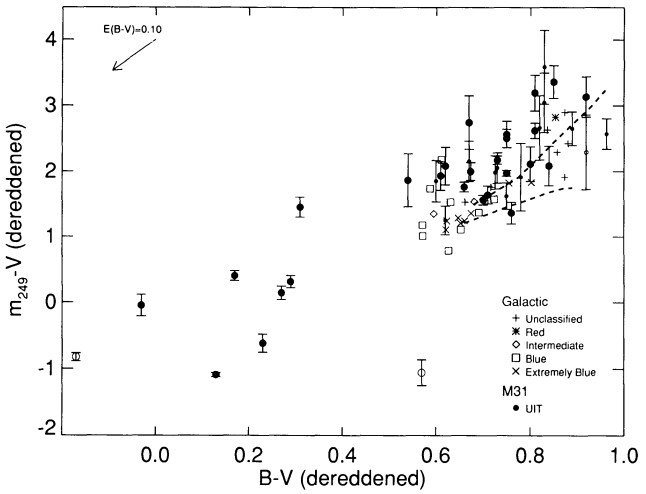

FIG. 8.—Intrinsic $(B-V)_0$ vs. intrinsic NUV color $(m_{249} - V)_0$. The symbols are as defined in Figure 5. The three M31 clusters with photographic colors are open symbols because of the large uncertainty of 0.4 mag in $B-V$. The heavy dashed lines are the predicted colors from the models of Buzzoni (1989) for an age of 15 Gyr and [Fe/H] ranging from -2.27 at the left-hand point to $+0.23$ at the right. The upper line is for a red horizontal branch, while the lower locus is for a blue horizontal branch morphology.

3.6. *Spectral Energy Distribution in the NUV to Visible Range*

Figure 8 is a comparison of the slope of the spectral energy distribution in the $B-V$ range with the slope from the NUV to visible. If the uncertain photographic $B-V$ color of Bo133 is confirmed, its location at (0.56, -1.06) on Figure 8 would indicate an anomalously strong NUV flux turnup. BoI notes that Bo133 is "bluish," which suggests that point should move left on Figure 8. In addition, van den Bergh (1964) includes the location of Bo133 in his OB association 13, which explains why the NUV image of Bo133 in Figure 3 shows a crowded field.

The broad bandpass (1800–3200 Å) of the UIT NUV filter permits both cool (~ 5000 K) main-sequence stars and hot ($\sim 10{,}000$ K) horizontal branch stars to contribute to an observed globular cluster flux. In order to assess the relative contribution of different stellar types to the NUV fluxes, the old stellar-population models of Buzzoni (1989) are integrated over the NUV filter bandpass. These model spectra account for the late stages in the life of low-mass stars such as the AGB and post-AGB phases and include the horizontal branch morphology as a free parameter. In the 15 Gyr models with a red HB morphology, most of the NUV flux longward of ~ 2500 Å arises from the main-sequence stars which are near the turnoff. The contribution of the main sequence in the models decreases with increasing metallicity due to the increased ultraviolet opacity. In the 15 Gyr models with a blue HB morphology, the blue HB can contribute significantly (33% of the total NUV flux) in metal-poor clusters and can dominate the NUV flux of metal rich clusters. Red and asymptotic giant branch stars and red HB stars never contribute a large fraction of the NUV flux. Because of their relatively brief lifetimes, hot post-AGB stars

are also minor contributors to the NUV flux. However, the high temperature post-AGB stars and related phases (post–early AGB, AGB-Manque) *can* provide a significant fraction of the flux in the FUV filter.

The heavy dashed lines in Figure 8 are the model colors for a 15 Gyr old population computed by Buzzoni (1989) from the Kurucz (1979) model atmospheres. The upper locus represents models with a red horizontal branch morphology and a metallicity varying from [Fe/H] = −2.27 at the left end of the line to [Fe/H] = 0.23 at the right end. The lower curve is for the same models with a blue horizontal branch. The two curves bracket most of the Galactic globulars. However, many of the M31 clusters have redder $m_{249} - V$ colors than predicted by any of the Buzzoni models, perhaps because the old Kurucz (1979) model atmospheres underestimated the ultraviolet opacity. To a first approximation, Figure 8 suggests that the M31 globular system consists of a coeval 15 Gyr system with a large spread in metallicities and horizontal branch morphology. However, the use of HB morphology as a free parameter may mask any true age spread among the M31 globulars. A more detailed analysis would consider the likely dependence of the HB morphology on the cluster age (Lee 1992).

4. SUMMARY

Using the lists of the Bologna group, vacuum-UV images from the UIT on the Astro-1 mission are searched for star clusters in two fields of 40′ diameter in M31. We identify 42 clusters on the NUV (2490 Å) frames but only ten on the FUV (1520 Å) frames. Approximate limiting magnitudes are $m_{249} \sim 19.4$ and $m_{152} \sim 18.3$ in our 286 to 583 s exposures. On the basis of their $m_{249} - V$ and $B-V$ colors, the clusters fall into two groups: (a) most are old globulars, comparable to those in our galaxy with intrinsic colors of $B-V > 0.5$ and $m_{249} - V > 1.0$; and (*b*) nine appear to be younger clusters, with $B-V < 0.4$ and $m_{249} - V < 1.0$.

In a comparison of the group (a) UV photometry with existing photometry of Galactic globulars from the *ANS* satellite, the M31 and Galactic globulars span approximately the same range of $(UV-V)$ color in both the near and far-UV. However, the M31 clusters tend to have redder UV colors at a given M_V, [Fe/H], or $(B-V)$ than the Galactic globulars, though such comparisons are probably dominated by selection effects.

A reevaluation of the existing *IUE* spectra of M31 clusters produces reasonable agreement with the UIT data in the NUV, but some published FUV fluxes from *IUE* should have been interpreted as upper limits. Fluxes obtained from our rocket prototype of UIT are also suspect. Overall, the UV fluxes of the red M31 clusters are not consistent with intermediate ages less than 5 Gyr, as some earlier studies had suggested. The predictions of the Buzzoni (1989) models for a 15 Gyr old population with a range of metallicity and HB morphology lie in the region of the observed NUV colors in Figure 8. The UIT data suggest that the M31 globular clusters are close counterparts of Galactic globulars.

We thank René Walterbos for providing supplemental data used in the preparation of Elson & Walterbos (1988) and Alberto Buzzoni for his evolutionary population synthesis models. Holland Ford encouraged us to initiate this work. Portions of this research were funded by NASA grants NAG5-1278 to the Space Telescope Science Institute and NAG5-700 and NAGW-2596 to the University of Virginia. The UIT instrument was funded under NASA Project Number 440-51-02.

REFERENCES

Barbero, J., Brocato, E., Cassatella, A., Castellani, V., & Geyer, E. H. 1990, ApJ, 351, 98
Battistini, P., Bònoli, F., Breccesi, A., Federici, L., Fusi Pecci, F., Marano, B., & Borngen, F. 1987, A&AS, 67, 447 (BoII)
Battistini, P., Bònoli, F., Breccesi, A., Fusi Pecci, F., Malagnini, M. L., & Marano, B. 1980, A&AS, 42, 357 (BoI)
Bohlin, R. C., Cornett, R. H., Hill, J. K., Hill, R. S., & Stecher, T. P. 1988, ApJ, 334, 657
Brodie, J. P., & Huchra, J. P. 1991, ApJ, 379, 157
Burstein, D., Bertola, F., Buson, L. M., Faber, S. M., & Lauer, T. R. 1988, ApJ, 328, 440
Burstein, D., Faber, S. M., Gaskell, C. M., & Krumm, N. 1984, ApJ, 287, 586
Buzzoni, A. 1989, ApJS,71, 817
Cacciari, C., Cassatella, A., Bianchi, L., Fusi-Pecci, F., & Kron, R. G. 1982, ApJ, 261, 77
Castellani, V., & Cassatella, A. 1987, in Exploring the Universe with the *IUE* Satellite, ed. Y. Kondo (Dordrecht: Reidel), 637
Cowley, A. P., & Burstein, D. 1988, AJ, 95, 1071 (CB)
Crampton, D., Cowley, A. P., Schade, D., & Chayer, P. 1985, ApJ, 288, 494
Crenshaw, D. M., Breugman, O. W., & Norman, D. J. 1990, PASP, 102, 463
Crotts, A. P. S., Kron, R. G., Cacciari, C., & Fusi-Pecci, F. 1990, AJ, 1000, 141
de Boer, K. 1985, A&A, 142, 321
———. 1987, in IAU Colloq. 95, The Second Conference on Faint Blue Stars, A. G. Davis Philip, D. S. Hayes, & J. W. Liebert (Schenectady: L. Davis Press), 95
Djorgovski, S., & Piotto, G. 1993, in The Globular Cluster–Galaxy Connection, ed. J. P. Brodie & G. H. Smith (San Francisco: ASP), in press
Elson, R. A. W., & Walterbos, R. A. M. 1988, ApJ, 333, 594 (EW88)
Frogel, J. A., Persson, S. E., & Cohen, J. G. 1980, ApJ, 240, 785
Greggio, L., & Renzini, A. 1990, ApJ, 364, 35
Harris, W. E., & Racine, R. 1979, ARA&A, 17, 241
Hodge, P. 1992, The Andromeda Galaxy (Dordrecht: Kluwer)
Huchra, J. P., Staufler, J., & van Speybroeck, L. 1982, ApJ, 259, L57
Huchra, J. P., Brodie, J. P., & Kent, S. M. 1991, ApJ, 370, 495
Kinney, A. L., Bohlin, R. C., & Neill, J. D. 1991, PASP, 103, 694
Kron, G. E., & Mayall, N. U. 1960, AJ, 65, 581
Kurucz, R. L. 1979, ApJS, 40, 1
———. 1992, in IAU Symp. 149, The Stellar Populations of Galaxies, ed. B. Barbuy & A. Renzini (Dordrecht: Kluwer), 225
Lasker, B. M., Sturch, C. R., McLean, B. J., Russell, J. L., Jenkner, H., & Shara, M. M. 1990, AJ, 99, 2019
Lee, Y-W. 1992, PASP, 104, 798
Lee, Y-W., Demarque, P., & Zinn, R. 1990, ApJ, 350, 155
O'Connell, R. W. 1983, in Highlights of Astronomy, ed. R. M. West (Dordrecht: Reidel), 147
———. 1993, in The Globular Cluster–Galaxy Connection, ed. J. P. Brodie & G. H. Smith (San Francisco: ASP), in press
Rich, R. M., Minniti, D., & Liebert, J. W. 1993, ApJ, 406, 63
Rood, R. T., & Crocker, D. A. 1989, in IAU Colloq. 111, The Use of Pulsating Stars in Fundamental Problems of Astronomy, ed. E. G. Schmidt (Cambridge: Cambridge Univ. Press), 103
Sargent, W. L. W., Kowal, C. T., Hartwick, F. D. A., & van den Bergh, S. 1977, AJ, 82, 947
Schaller, G., Schaerer, D., Meynet, G., & Maeder, A. 1992, A&AS, 96, 269
Searle, L., & Zinn, R. 1978, ApJ, 225, 357
Seaton, M. 1979, MNRAS, 107, 73
Sharov, A. S., & Lyuty, V. M. 1983, Ap&SS, 90, 371
———. 1985, Soviet Astron. Lett., 11, 248
Sharov, A. S., Lyuty, V. M., & Esipov, V. F. 1984, Soviet Astron. Lett., 10, 243
———. 1987, Soviet Astron. Lett., 13, 270
Sharov, A. S., Lyuty, V. M., & Ikonnikova, N. P. 1992, Soviet Astron. Lett., 18, 41
Spinrad, H., & Schweizer, F. 1972, ApJ, 171, 403
Stecher, T. P., et al. 1992, ApJ, 395, L1
Tripicco, M. J. 1989, AJ, 97, 735
van Albada, T. S., de Boer, K. S., & Dickens, R. J. 1981, MNRAS, 195, 591
van den Bergh, S. 1964, ApJS, 9, 65